

A MULTI-CHANNEL WIRELESS RESPIRATORY AND HEART SOUNDS
ACQUISITION AND PROCESSING SYSTEM

by

Onur Yusuf Çınar

B.S., Electrical and Electronics Engineering, Boğaziçi University, 2015

Submitted to the Institute for Graduate Studies in
Science and Engineering in partial fulfillment of
the requirements for the degree of
Master of Science

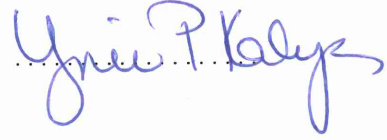
Graduate Program in Electrical and Electronics Engineering
Boğaziçi University

2019

A MULTI-CHANNEL WIRELESS RESPIRATORY AND HEART SOUNDS
ACQUISITION AND PROCESSING SYSTEM

APPROVED BY:

Prof. Dr. Z. Yasemin Kahya
(Thesis Supervisor)



Prof. Dr. Oğuzhan Çiçekoğlu



Assist. Prof. İpek Şen



DATE OF APPROVAL: 29.07.2019

ACKNOWLEDGEMENTS

Primarily, I am grateful to my master thesis advisor, Prof. Dr. Yasemin Kahya for her endless support throughout my study who gives me moral and material support at Boğaziçi University, Lung Acoustic Laboratory (LAL) from the beginning to the end of my master thesis process. Moreover, I would like to thank my evaluation committee members Prof. Dr. Oğuzhan Çiçekođlu and Asst. Prof. İpek Ően for their participations and valuable reviews.

I would like to thank my lifelong teacher, wise woman, my mother Gülhan Çınar, and also my permanent promoters, my father Köksal Çınar and my sister Seda Çınar, for their unending support through all my life and for being subjects in my medical measurements. Without them, I would not be able to do what I have achieved in my life.

Moreover, I would also like to thank my friends, Mert Can Çinka, Volkan Dođan and Nirva Peřtemalciyan for their moral support through my master thesis period, who promoted and encouraged me more than they thought.

ABSTRACT

A MULTI-CHANNEL WIRELESS RESPIRATORY AND HEART SOUNDS ACQUISITION AND PROCESSING SYSTEM

Methods and diagnostic tools used in medical examinations of cardiac and respiratory diseases have not changed significantly since they have been invented. Auscultation is an advantageous way for physical examination due to the fact that it is a noninvasive method for patients, however, acoustic stethoscope as a diagnostic tool, is inadequate and not open for improvement because medical doctors can not record, share and standardize their patients' pulmonary and cardiac sounds.

With our new digital and wearable sound acquisition and processing system proposed in this thesis, up to 6 channels (4 of them placed on the posterior chest and 2 of them placed on the anterior chest region on the patient's body) pulmonary and cardiac sounds can be stored simultaneously and they can be transferred to a mobile or console application via Bluetooth connectivity that includes not only auscultation signals but also valuable information about diagnosis that consists of calculation of percentile frequencies of each channel on embedded side.

Real time auscultation of each channel one by one with 3.5 mm headphone connection, storing multiple records of multiple patients on the same device, extracting respiratory flow phase via not only a conventional method, pneumotachograph, but also with a newly designed stretch sensor interface that is suitable for wearable devices are available features within this device.

ÖZET

ÇOK KANALLI KABLOSUZ SOLUNUM VE KALP SESLERİ TOPLAMA VE İŞLEME SİSTEMİ

Solunum ve kalp hastalıklarının tanısında kullanılan methodlar ve araçlar, icat edildiklerinden beri büyük bir değişikliğe uğramadılar. Oskültasyon, insan vücuduna zarar vermemesi sebebiyle kullanışlı bir yöntemdir, ancak akustik stetoskopların kendine ait özelliklerinin yetersiz olması ve gelişime açık olmamasından ötürü medikal doktorlar, hastalarının solunum ve kalp seslerini kaydedemiyor, paylaşamıyor ve standart hale getiremiyorlar.

Bu tezde sunulan yeni, sayısal ve giyilebilir ses toplama ve işleme sistemi sayesinde, 6 kanala kadar (4 tanesi sırt bölgesinde, 2 tanesi göğüs bölgesinde) solunum ve kalp sesi kaydedilebiliyor ve bir mobil cihaza ya da bir bilgisayar uygulamasına Bluetooth bağlantısı vasıtasıyla hem oskültasyon sinyalleri hem de teşhis için yardımcı olabilecek yüzdeli frekanslar hesaplanarak gönderilebiliyor.

Sistemin temel işlevlerinin yanı sıra sahip olduğu özellikler, her kanalın ses sinyallerini 3.5 mm'lik kulaklık girişi sayesinde canlı olarak dinleyebilmek, ve solunum fazı bilgisini, geleneksel bir yöntem olan fnömotakografin yanı sıra yeni tasarlanan gerginlik sensörü ile alabilmektir.

TABLE OF CONTENTS

ACKNOWLEDGEMENTS	iii
ABSTRACT	iv
ÖZET	v
LIST OF FIGURES	viii
LIST OF TABLES	xii
LIST OF SYMBOLS	xiv
LIST OF ACRONYMS/ABBREVIATIONS	xv
1. INTRODUCTION	1
1.1. Background	1
1.2. Motivation and Aim	3
1.3. Thesis Outline	5
2. SYSTEM ARCHITECTURE	7
3. MAIN BOARD	9
3.1. Microcontroller	14
3.2. Display, Button and Headphone Connection	16
3.3. Bluetooth Connectivity	18
3.4. Memory	21
3.4.1. IC Memories	21
3.4.2. microSD Card	23
3.5. Other Features	24
3.5.1. Power Management	24
3.5.2. Stretch Sensor	25
3.5.3. Pneumotachograph and Pulse Oximeter	26
3.5.4. Ambient Noise Cancellation	27
4. CAPSULE BOARD	29
4.1. Instrumentation Amplifier	35
4.2. Pulmonary Sound Filter	38
4.2.1. High-Pass Filter	38
4.2.2. Low-Pass Filter	41

4.3. Cardiac Sound Filter	44
4.4. Analog-to-Digital Conversion	46
4.5. Other Features	47
4.5.1. Power Management	47
4.5.2. Accelerometer	48
5. EMBEDDED SOFTWARE	49
6. PERCENTILE CALCULATION ALGORITHM	52
7. EXPERIMENTS AND RESULTS	54
8. CONCLUSION	58
REFERENCES	60
APPENDIX A: TECHNICAL DRAWING OF THE MICROPHONE CAPSULES	62
APPENDIX B: FAST FOURIER TRANSFORM ALGORITHM [16]	63
APPENDIX C: THE DATASHEET OF POM-2245L-C33R MICROPHONE	65
APPENDIX D: THE COMPONENT LIST OF THE MAIN BOARD	66
APPENDIX E: THE COMPONENT LIST OF THE CAPSULE BOARD	69

LIST OF FIGURES

Figure 1.1.	Early Stethoscopes.	1
Figure 1.2.	Fluctuating Frequency Response of a Stethoscope [5].	2
Figure 1.3.	Four Predefined Regions for Recording.	4
Figure 2.1.	The System Architecture.	7
Figure 3.1.	Main Board Architecture.	9
Figure 3.2.	Main Board Channel Localization.	11
Figure 3.3.	Main Board Enclosure.	11
Figure 3.4.	Main Board PCB.	12
Figure 3.5.	Top and Bottom Sides of Manufactured PCB of the Main Board.	12
Figure 3.6.	The Schematics of the Main Board.	13
Figure 3.7.	The Schematics of Microcontroller Part.	15
Figure 3.8.	The Schematics of Audio Part.	16
Figure 3.9.	The Schematics of Bluetooth Part.	18
Figure 3.10.	The Schematics of USB Connection Part.	20

Figure 3.11.	The Schematics of Parallel Memory Part.	22
Figure 3.12.	The Schematics of Serial Memory Part.	22
Figure 3.13.	The Schematics of microSD Card Part.	23
Figure 3.14.	The Schematics of Power Management Part.	24
Figure 3.15.	The Schematics of Power Distribution Part.	25
Figure 3.16.	The Resistive Stretch Sensor [12].	26
Figure 3.17.	The Connector of Pneumotachograph.	26
Figure 3.18.	The Working Scheme of Pulse Oximeter [13].	27
Figure 3.19.	The I2C Interface of Pulse Oximeter.	28
Figure 3.20.	The Schematics of Ambient Noise Cancellation and Respiratory Flow Phase Detection Circuit.	28
Figure 4.1.	The General Architecture of the Capsule Board.	29
Figure 4.2.	The Layout of the Capsule Board.	30
Figure 4.3.	The PCB Products of the Capsule Board.	31
Figure 4.4.	The Final Products of the Capsule Boards.	31
Figure 4.5.	The Final Product of the Wearable Device with Pillow Option. . .	32

Figure 4.6.	The Final Product of the Wearable Device with Corset Option. . .	32
Figure 4.7.	The Block Diagram of General Supply and Reference Voltages Generation Scheme.	33
Figure 4.8.	The Block Diagram of Local Supply and Reference Voltages Generation Scheme.	34
Figure 4.9.	The Schematics of Capsule Board.	35
Figure 4.10.	The Schematics of Instrumentation Amplifier.	36
Figure 4.11.	The Schematics of Digital Potentiometer.	37
Figure 4.12.	The Schematics of High Pass Filter for Pulmonary Sound.	38
Figure 4.13.	The Circuit Diagram of Sallen Key Topology for High Pass Filter [14].	39
Figure 4.14.	The Schematics of Low Pass Filter for Pulmonary Sound.	41
Figure 4.15.	The Circuit Diagram of Sallen Key Topology for Low Pass Filter [14].	42
Figure 4.16.	The Frequency Response of the Band Pass Filter for Pulmonary Sound.	43
Figure 4.17.	The Schematics of Band Pass Filter for Cardiac Sound.	44
Figure 4.18.	The Frequency Response of the Band Pass Filter for Cardiac Sound.	46
Figure 4.19.	The Schematics of Analog to Digital Converter IC.	47

Figure 4.20.	The Schematics of Power Management on Capsule Board.	47
Figure 4.21.	The Schematics of Accelerometer.	48
Figure 5.1.	The Main Flow Diagram of the Embedded Code.	49
Figure 6.1.	The Percentile Frequencies of a PSD.	53
Figure 7.1.	The Respiratory Sound Waveforms of 4 Channels of Measurement 1.	54
Figure 7.2.	The Respiratory Sound Waveforms of 4 Channels of Measurement 2.	55
Figure 7.3.	The Respiratory Sound Waveforms of 4 Channels of Measurement 3.	55
Figure A.1.	Technical Drawing of the Microphone Capsules.	62
Figure C.1.	The Datasheet of POM-2245L-C33-R Electret Microphone [18].	65

LIST OF TABLES

Table 4.1.	Bessel Filter Table for 6th Order Filter Design	40
Table 4.2.	Cutoff Frequency Table for 6th Order Bessel Filter Design	40
Table 4.3.	Component Values for 6th Order Bessel Filter Design	40
Table 4.4.	Butterworth Filter Table for 8th Order Filter Design	42
Table 4.5.	Component Values for 8th Order Butterworth Filter Design	43
Table 4.6.	Butterworth Filter Table for 4th Order Filter Design	45
Table 4.7.	Component Values for 4th Order Butterworth High Pass Filter Design	45
Table 4.8.	Component Values for 4th Order Butterworth Low Pass Filter Design	45
Table 5.1.	The Package Mechanism of Data Transmission	50
Table 7.1.	The Information Table of Healthy Subjects	54
Table 7.2.	Percentile Frequencies Table of Channel 1 for Each Measurements	56
Table 7.3.	Percentile Frequencies Table of Channel 2 for Each Measurements	56
Table 7.4.	Percentile Frequencies Table of Channel 3 for Each Measurements	56
Table 7.5.	Percentile Frequencies Table of Channel 4 for Each Measurements	57

Table D.1.	The IC Table of the Main Board	66
Table D.2.	The Resistor Table of the Main Board	67
Table D.3.	The Capacitor Table of the Main Board	68
Table E.1.	The IC Table of the Capsule Board	69
Table E.2.	The Resistor Table of the Capsule Board	70
Table E.3.	The Capacitor Table of the Capsule Board	71

LIST OF SYMBOLS

f_{25}	The frequency covers 25% of Power Spectral Density
f_{50}	The frequency covers 50% of Power Spectral Density
f_{75}	The frequency covers 75% of Power Spectral Density
f_{90}	The frequency covers 90% of Power Spectral Density



LIST OF ACRONYMS/ABBREVIATIONS

3D	Three Dimensional
ADC	Analog to Digital Converter
AT	ATtention
BP	Band Pass
CAD	Computer Aided Design
CMRR	Common Mode Rejection Ratio
DC	Direct Current
EDR	Enhanced Data Rate
FAT	File Allocation Table
FFT	Fast Fourier Transform
GPIO	General Purpose Input Output
HAL	Hardware Abstraction Layer
HP	High Pass
I2C	Inter-Integrated Circuit
IC	Integrated Circuit
ID	Identification
k-NN	k-Nearest Neighborhood
LP	Low Pass
LQFP	Low Profile Quad Flat Pack
LSB	Least Significant Bit
MISRA C	Motor Industry Software Reliability Association C
OPAMP	Operational Amplifier
PLL	Phase Locked Loop
PCB	Printed Circuit Board
PSD	Power Spectral Density
PSRR	Power Supply Rejection Ratio
QSPI	Quad Serial Peripheral Interface
RC	Resistor Capacitor

RFI	Radio Frequency Interference
RCA	Radio Corporation of America
RTS	Request to Send
RX	Receiver
SDIO	Secure Digital Input Output
SDMMC	Secure Digital Multi Media Card
SPI	Serial Peripheral Interface
SWD	Serial Wire Debug
TIM	Timer
TX	Transmitter
UART	Universal Asynchronous Receiver Transmitter
USB	Universal Serial Bus

1. INTRODUCTION

1.1. Background

Auscultation (based on the Latin verb *auscultare* "to listen") is listening to the internal sounds of the body, usually using a stethoscope. Auscultation is performed for the purpose of examining the circulatory and respiratory systems (heart and breath sounds), as well as the gastrointestinal system (bowel sounds) [1]. Before the invention of the stethoscope, clinicians' ear was the single diagnostic instrument that was placed on their patient's body in order to listen to pulmonary and cardiac sounds, and to determine their medical conditions depending upon their hearing capacity and previous experiences. With the invention of the stethoscope, in 1816 by René Laennec at the Necker-Enfants Malades Hospital in Paris, France, which was similar to an ear trumpet that amplifies the sound via acoustic gain, the volume of the acquired sound has been increased [2].

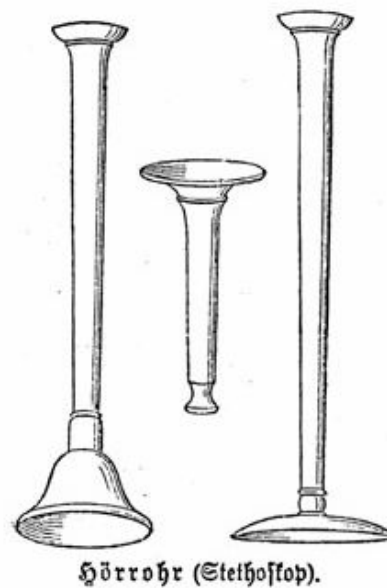


Figure 1.1. Early Stethoscopes.

Due to the gain enhancement of stethoscopes, medical doctors use acoustic stethoscopes during the physical examination of their patients in order to diagnose their diseases and to follow up their medical conditions. Moreover, the methods and tools for health examinations including pulmonary and cardiac sounds have not changed significantly yet since the first invention of the stethoscope. At the same time, the diagnostic method mentioned above does have several deficiencies.

One of the main drawbacks of acoustic stethoscopes is about their limited frequency response that attenuates frequencies above 112 Hz [3], whereas the human ears are not very sensitive to the frequencies below this value and the spectrum of respiratory sounds recorded on the chest extends up to 2000 Hz for normal breath sounds and 6000 Hz for pathological cases [4].

Another disadvantage of the stethoscope is that its frequency spectrum is fluctuating [5]. If an objective and standardized medical diagnostic is desired, the frequency response of a stethoscope should be flat which means that the magnitude of each component on the transfer function must be the same.

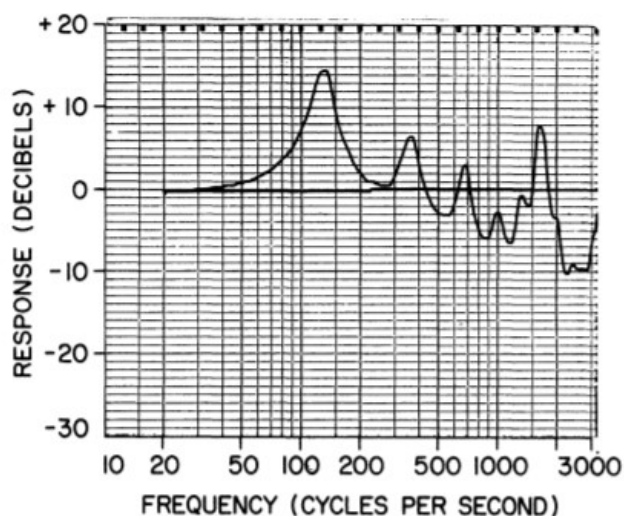


Figure 1.2. Fluctuating Frequency Response of a Stethoscope [5].

Besides the deficiencies due to the limitations of mechanical structure of stethoscopes, the method itself is problematic which means that the pulmonary or cardiac sound acquired from a patient, is not digital. This results in the problem that medical doctors can not listen one record more than once, can not share it with their professors to consult or students to teach them, and also computerized techniques are not applicable that could be available if pulmonary and cardiac sounds were digitized. Computerized techniques are available because there are predefined patterns of common respiratory sound deficiencies such as wheeze, fine crackle and coarse crackle in the literature [6].

1.2. Motivation and Aim

Because of the deficiencies and imperfections of the acoustic stethoscopes mentioned above, a wearable device that is a multi-channel respiratory and heart sound data acquisition and processing system is designed and realized in this thesis.

According to the previous studies, master theses and research at Bogazici University, Lung Acoustic Laboratory (LAL) [7], [8], there are 4 preferred channels as can be seen in Figure 1.3 on the posterior chest of a patient in order to record and process respiratory sounds. As a general procedure, we assume that one inhalation and exhalation duration of an ordinary subject takes approximately around five seconds that guarantee two respiration cycles if we record ten-second sessions for each channel. In addition to these four channels, two new channels have been added so as to extend respiratory sound research with new regions on the chest region and also study on cardiac sounds. In order to produce an easy-to-use device, a mechanical and wearable design has been completed which includes four channels with adjustable location options in a corset and pillow as two alternatives.

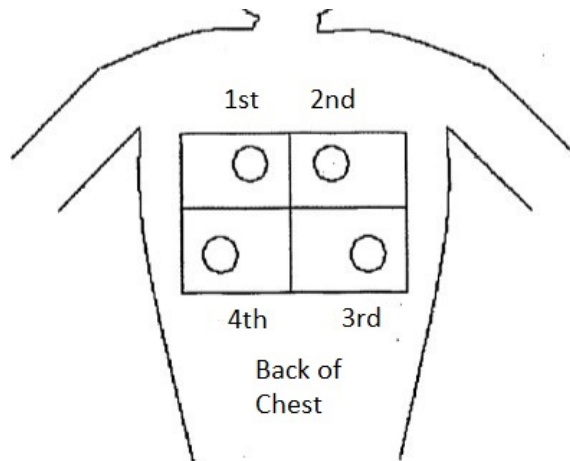


Figure 1.3. Four Predefined Regions for Recording.

In addition to the band pass analog filter that has a frequency response between 80 Hz and 2000 Hz which is suitable for pulmonary sound studies [7], in this device, there is another analog filter which has a frequency response between 30 Hz and 500 Hz for cardiac sound studies [9]. Thanks to digital switch, either one of the pulmonary or cardiac sound filters can be selected digitally. This feature paves the way to change the frequency response of the filter with commands via wireless connectivity, and also allows us to record pulmonary and cardiac sounds in the single record session by changing filters rapidly, because sampling and conversion time is much less than the time between consecutive sampling in our case. Therefore, it is available to record one session and to obtain respiratory and heart sounds of a subject at the same time.

Because of the fact that patients may include child, adult, slim or fat persons, adjustable gain of volume for each channel is available thanks to digital potentiometers. In addition to volume adjustment, as mentioned above, adjustable channel localization is advantageous for patients with various body sizes which results in the fact that the location and volume level of each channel can be configured easily with this wearable device.

Moreover, via headphone jack connection and headphone amplifier, each channel can be auscultated via 3.5 mm headphone. Channels can be switched via a button on the device and channel number is indicated on 7-segment display to show which channel is listening, and also volume level can be controlled via volume potentiometer on the device.

Diagnosis of respiratory diseases is not only related to the number of adventitious sound patterns that are mentioned above as predefined respiratory sound deficiencies but also the localization in the time domain. It means that the existence of one disordered pattern at the beginning or at the end of inspiration may be the result of different medical conditions [7]. Furthermore, respiratory flow phase is observed by medical doctors while examining their patients and they do not need an additional data about the synchronization of pulmonary sounds and respiratory phase while diagnosing. However, it is a wearable device and people can use it on their own, so a respiratory phase detection is required for processing acquired sounds to synchronize them. In order to solve this problem, three alternatives are presented such as pneumotachograph, a resistive stretch sensor design that is suitable for wearable devices and also an accelerometer for respiratory phase detection in this thesis.

Besides the fact that electronic circuit design consists of analog and digital circuits, wearable and mechanical design, and diversified respiratory phase detection methods, there is also an embedded software part that controls whole operation of the system and also calculates percentile frequencies for each channel. Its low level operation and algorithms that are helpful for diagnosis will be mentioned in more detail in the corresponding sections.

1.3. Thesis Outline

In Chapter 2, the system architecture and the main board are explained that include a microcontroller, Bluetooth connectivity, headphone and pneumotachograph interfaces, stretch sensor input and its circuitry, different storage options as serial, parallel memories and microSD Card, and in order to combine all of these components

in a single board, its schematic and PCB design. For future purposes, there is also a pulse oximeter connection that is mentioned in this chapter which will be helpful especially for cardiac sound studies.

Chapter 3 gives the details about capsule board that is the analog preprocessing and acquisition part of the system. Most of the analog part of the system belongs to capsule board which is explained in this chapter. There is a microphone interface, one instrumentation amplifier, two different band pass filters with selection option, and an ADC IC in this circuitry. For future purposes, an additional microphone for noise cancellation and an accelerometer for respiratory phase detection are available.

Chapter 4 covers embedded part of the system that includes main flow diagram of the system, Bluetooth connectivity and lossless data transmission procedure, simultaneous data acquisition from up to 6 capsule boards and SDIO protocol with microSD Card.

Chapter 5 includes percentile frequencies algorithm that runs on the microcontroller which consists of low level FFT calculation and results in four parameters f_{25} , f_{50} , f_{75} and f_{90} for each channel.

Chapter 6 is the conclusion section of the thesis with results and future improvements.

2. SYSTEM ARCHITECTURE

As mentioned before, it is a complete system that not only includes wearable and mechanical design in order to fit patient's body, electronic circuit design which involves analog and digital circuitries, but also their production as a prototype. Moreover, there are also a mobile application to command the system and receive responses from the device and an embedded software to fulfill all operations.

The system architecture can be seen in Figure 2.1.

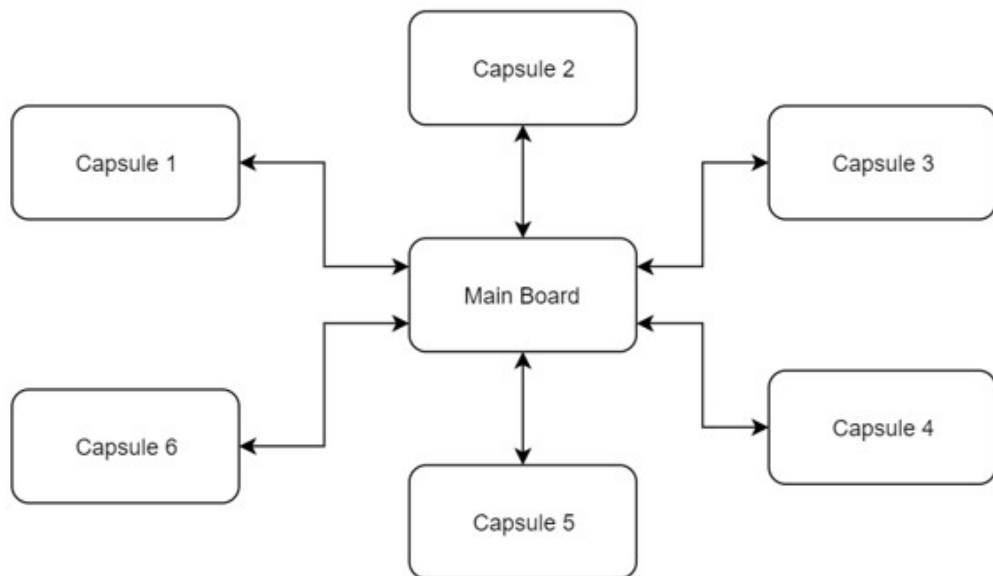


Figure 2.1. The System Architecture.

At the beginning of the design process, there were two options for system architecture. One of them is using a single ADC on the main board for up to 6 channels in order to convert analog signals to digital for each channel that are coming from each capsule which are placed on different regions on patient's body. Another option is that each capsule circuitry has its own ADC and main board reads only ADC conversion

values via SPI protocol from each channel.

The former option does have a basic disadvantage such as all analog signals coming from different capsules must travel at least 15 - 20 cm through cable so as to reach main board and ADC for conversion. This results in the fact that all incoming signals are vulnerable to noise that is coming from several sources from outside. It is also impractical to use a shielded coaxial cable in order to eliminate extraneous noise because of the input connector type of our selected microphones and the desire to make a small device.

Therefore, the latter option is better because if all analog-to-digital conversion can be fulfilled in their own PCBs for each capsule, the signal transmitted via cable becomes digital. This means that by using the advantageous feature of digital signals against analog signals that are being more immune to noise, the incoming analog signals can be protected. For this reason, the noise immunity issue is the key reason of system architecture design as a distributed network.

As a result, according to the necessities, up to 6 channels can be connected to the main board and via connection indicators, microcontroller adjusts itself as to which channels should be read and processed.

3. MAIN BOARD

The general architecture of the main board can be seen in Figure 3.1.

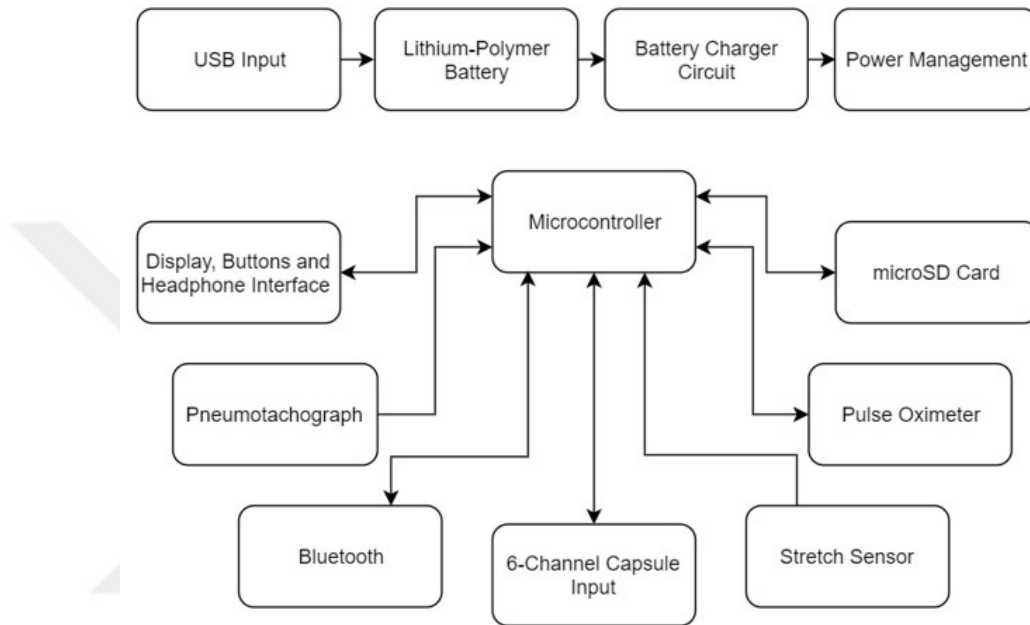


Figure 3.1. Main Board Architecture.

In an overview of the system, there is a microcontroller at the center of the board, and its peripherals are connected to other ICs and sensors. The circuit is powered by a Lithium-Polymer battery that is rechargeable via USB and a battery charger circuit. Headphone interface with its controller and indicator which are buttons and a 7-segment display, respectively, are placed on the main board. There is a pneumotachograph connection that is an RCA connector. Bluetooth connectivity with Bluetooth 2.0 module is available for receiving commands from a mobile device as well as for transmitting samples acquired from each channel and results of calculations to a mobile device.

There are also a stretch sensor circuitry, an I2C interface for pulse oximeter connection, a microSD Card circuitry and its connector for very large memory requirements, and 6 channel capsule connectors placed on the main board.

The PCB of the main board is designed as 4-layer PCB due to two significant reasons. One of them is that there are lots of connections between the 144-pin microcontroller and its peripherals, so PCB drawing becomes easier if 4-layer is selected. Another reason is more important than the previous one because if 4-layer PCB production is available, top and bottom layers can be drawn as ground plane. Then, if the circumference of the circuit is filled with vias that connect bottom and top layers, the main board acts as a Faraday Cage which protects the traces on the inner two layers inside the board from incoming noise from outside. All soldering pads are gold immersed that makes soldering process easier and also reduce junction resistance.

For the sake of easier wearable design and shorter the lengths of cables between the main and the capsule boards, the main board is placed at the center of the wearable textile. 4 main capsule and 2 extension capsule connectors are placed on the nearest region according to the location of each channel on the patient's body as shown in Figure 3.2. in order to shorten the length of cables as much as possible.

Its mechanical enclosure that is designed in a CAD tool and produced via a 3D printer, and the PCB of main board is shown in Figure 3.3. and Figure 3.4., respectively.

The bottom and top layers of the manufactured 4-layer, gold immersed PCB of the main board can be seen in Figure 3.5.

The schematics of the main board can be seen in large scale in Figure 3.6., and the rest of this chapter covers each part of the main board in detail.

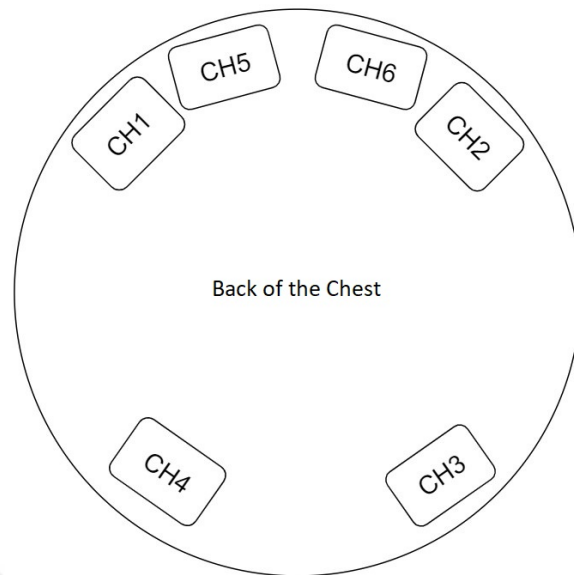


Figure 3.2. Main Board Channel Localization.

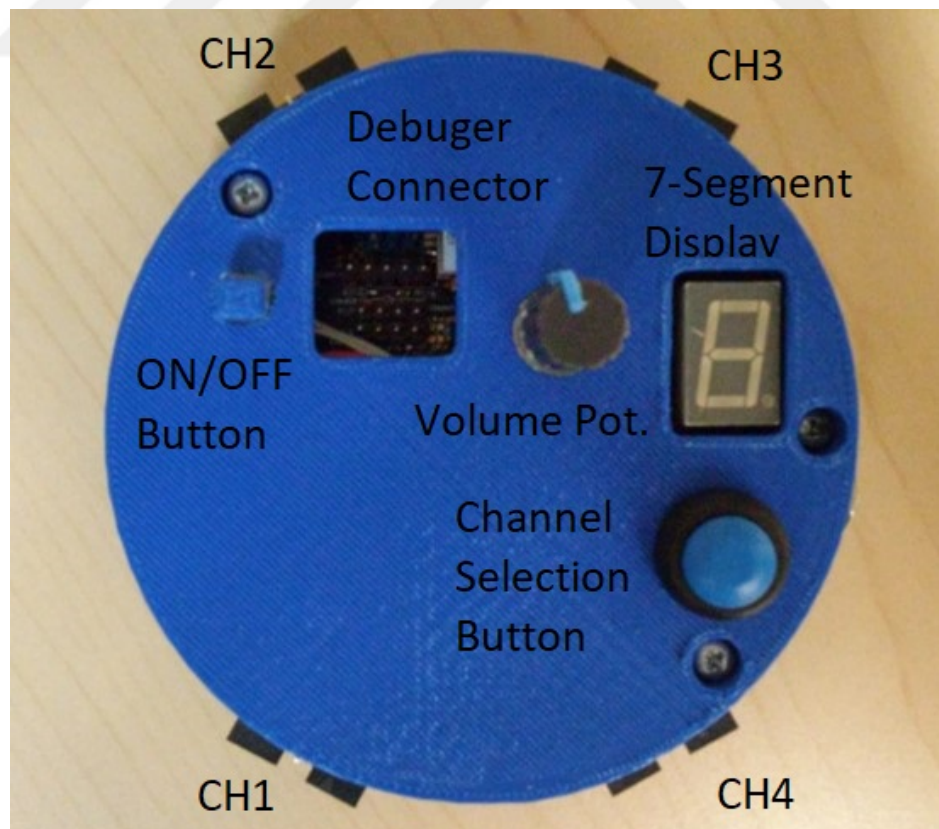


Figure 3.3. Main Board Enclosure.

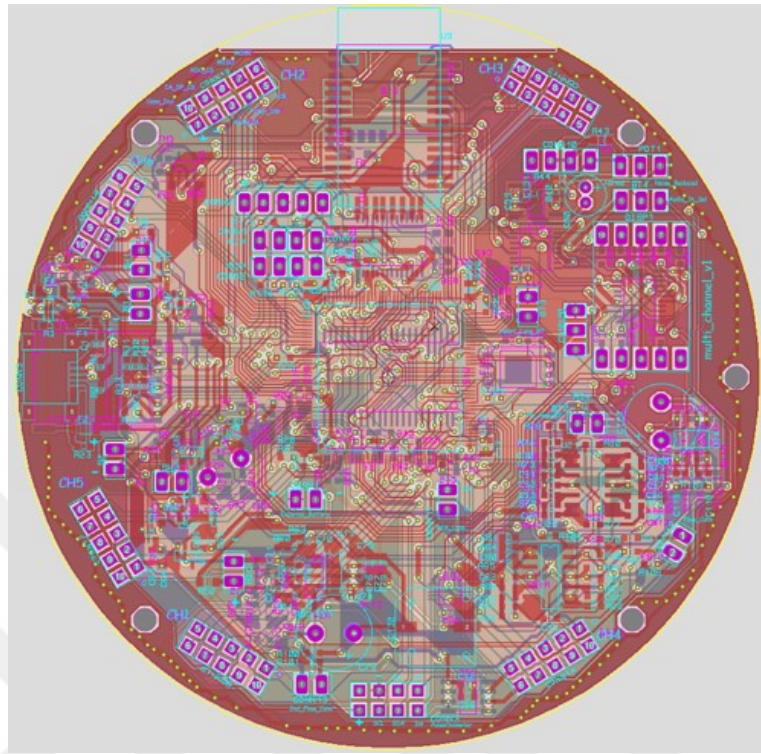


Figure 3.4. Main Board PCB.

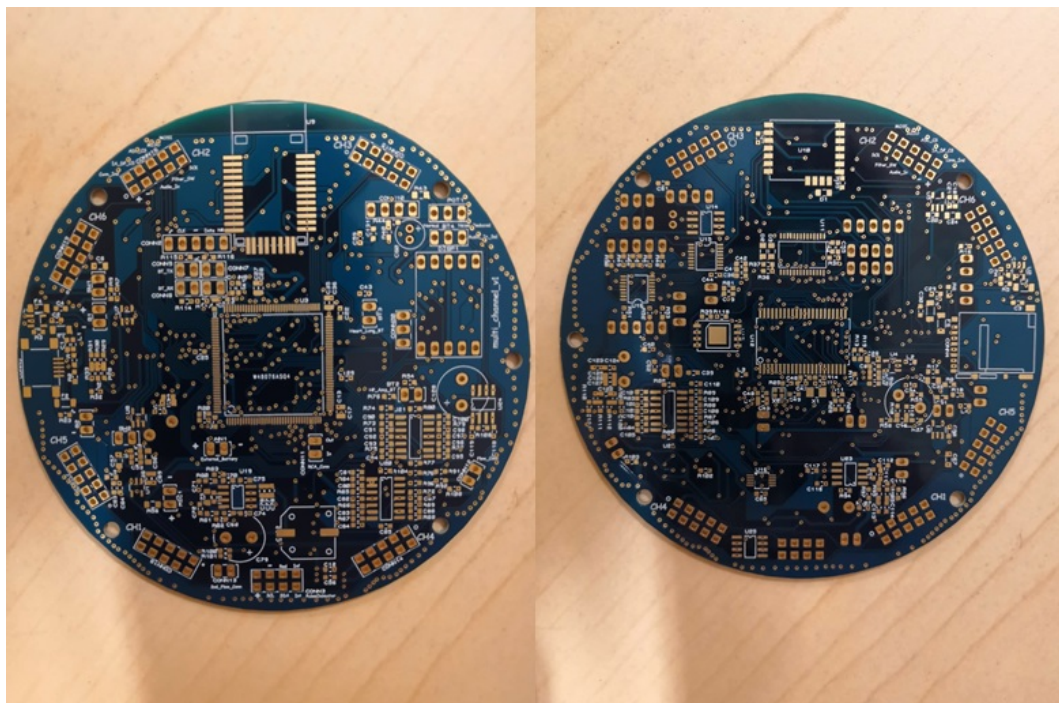


Figure 3.5. Top and Bottom Sides of Manufactured PCB of the Main Board.

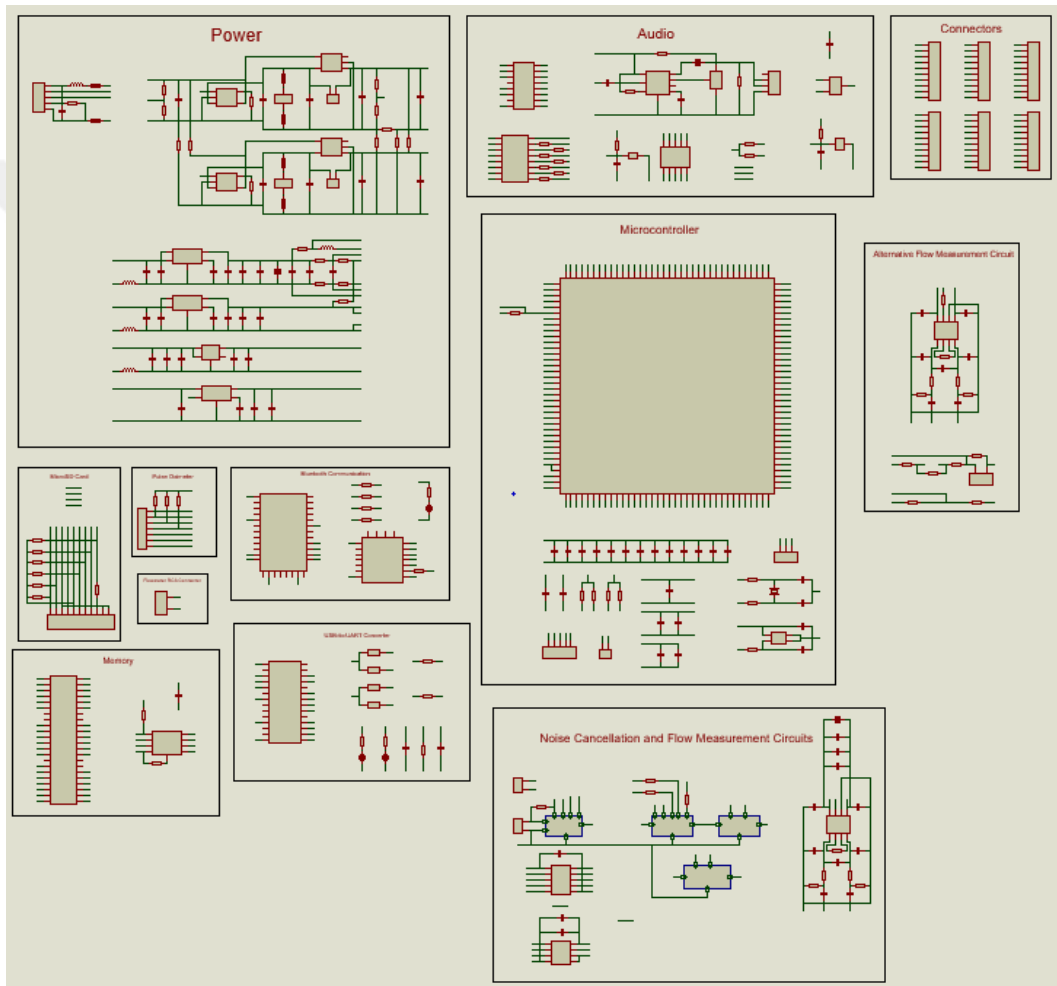


Figure 3.6. The Schematics of the Main Board.

3.1. Microcontroller

In order to collect data from up to 6 channels, to communicate with a mobile device via Bluetooth, to perform basic operations such as reading buttons and sensors or driving displays, and also to fulfill basic signal processing tasks, it is required to use a microcontroller in this system.

One of the ultimate microcontrollers on the market is used in the main board, that includes Cortex-M7 core (with double-precision floating point unit) running up to 216 MHz while reaching similar lower static power consumption which is STM32F777ZI [10]. This unit has 144 pins in LQFP package that is enough for the connections of 6 channels and also other peripherals. One of the main reasons to select STM32F777ZI is its large memory area, 512 kB, that is enough for recording up to 4 channels with 10 seconds record sessions. There is also an SDIO interface for easy communication with microSD Card.

Another main reason is that it has 6 SPI channels making the sampling of each channel simultaneously, which is crucial if the correlation of channels is to be studied. Finally, the last reason for selecting a microcontroller from ST Microelectronics is that they offer a firmware that is called Hardware Abstraction Layer which has been developed in compliance with the MISRA C guidelines and the demanding ISO/TS16949 standard for quality system management. HAL allows easy change from one microcontroller family to another and also makes development easier and reduces time spent.

The schematics of the microcontroller part can be seen in Figure 3.7.

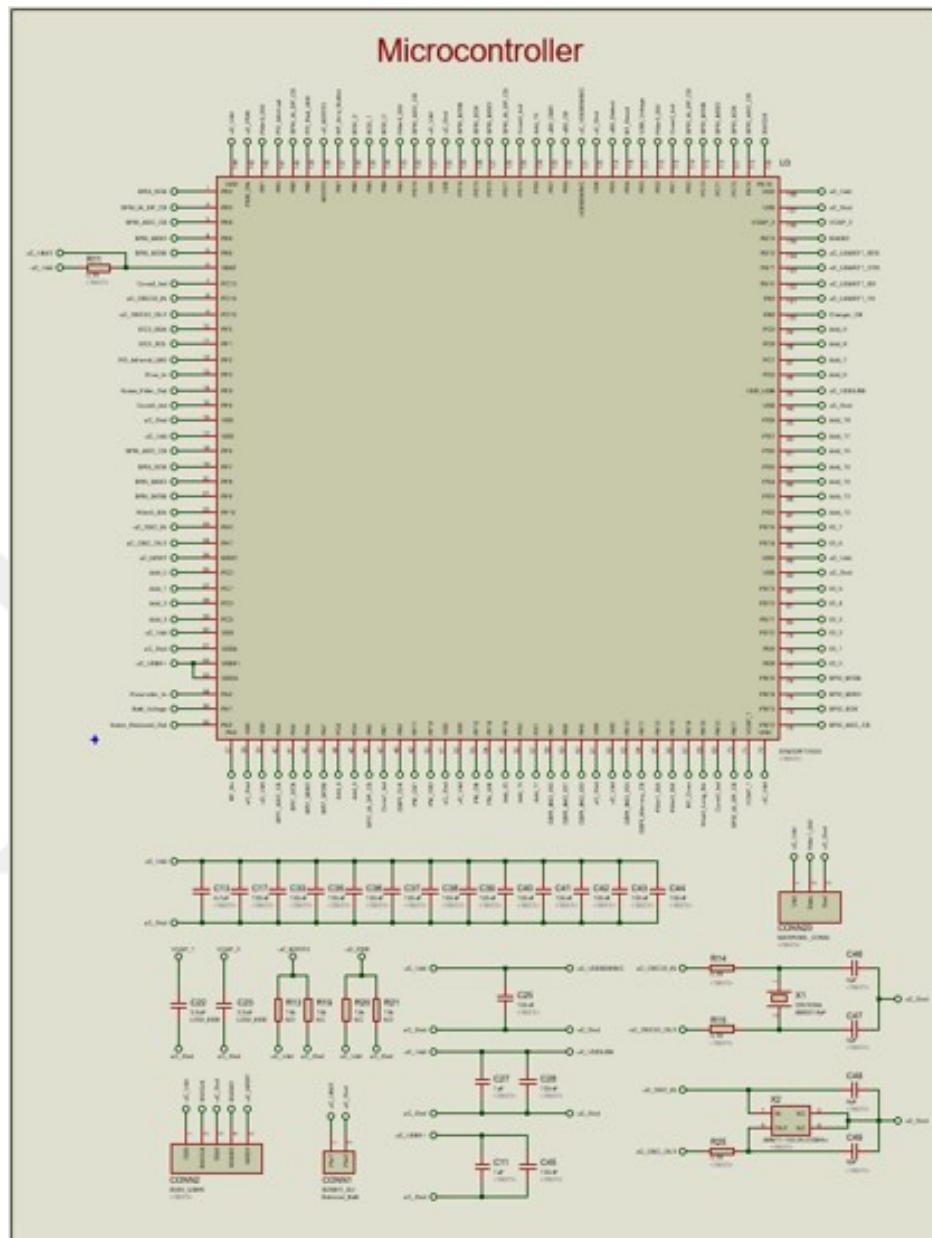


Figure 3.7. The Schematics of Microcontroller Part.

There is no free pin on microcontroller because every pin is connected with another component on the main board. There are decoupling capacitors that are placed as close to the supply pins of the microcontroller as possible and also across the reference voltage pins of ADC on the microcontroller itself. There is a debugger connector, SWD, in order to debug and also program the microcontroller. Two crystals are available, one of them is for 216 MHz with PLL function, and the other one is 32.768 kHz that is a subsidiary crystal if the first one fails, and also functional when sleep mode

is activated for low power consumption. There is also a Vbat pin to connect a battery for uninterrupted operation against the situation of failure of the main battery. After the general scheme of the schematics of the microcontoller, its embedded code is going to be explained in detail in its own chapter.

3.2. Display, Button and Headphone Connection

Because of the fact that this is a multi channel device and if it is intended to be used as a stethoscope and listen to the respiratory and cardiac sounds of a patient, channels should be selected. In order to perform this, a button, a 7-segment common anode display, a volume potentiometer and a 3.5 mm headphone jack are available which can be seen in Figure 3.3. By using the push button, channel selection has a circular order that means when the channel number reaches the maximum number, it turns back to the first one if push button is pressed one more time. Its schematic is shown in Figure 3.8.

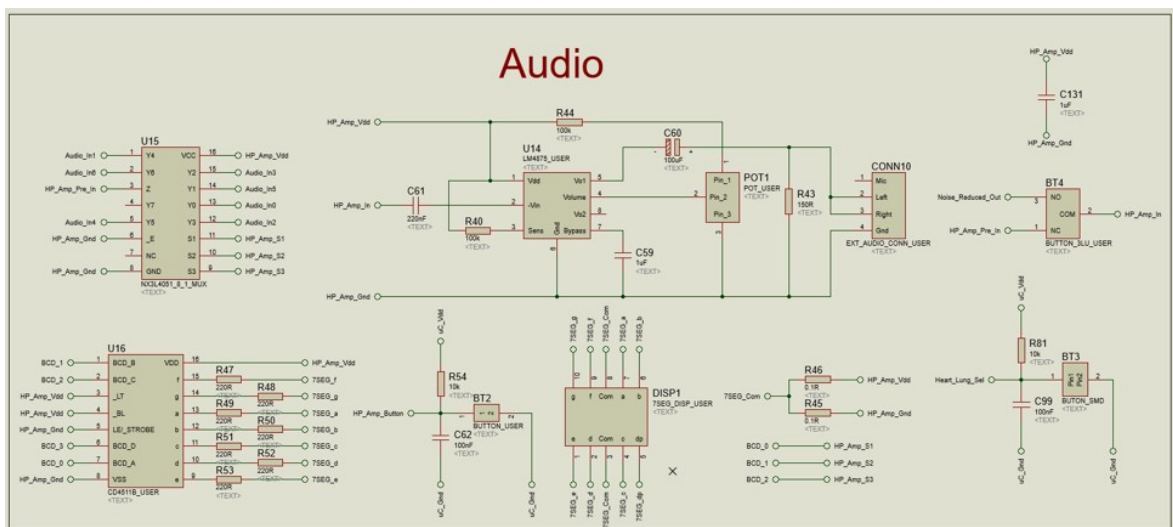


Figure 3.8. The Schematics of Audio Part.

Each capsule circuit sends different types of signals such as indication of a connection, SPI and I2C buses and so on. One of them is the raw audio signal that is amplified and filtered and transmitted to main board to be listened via headphone

connection. In an effort to select one channel to listen, there is a digital switch which is actually a multiplexer, NX3L4051 from NXP Semiconductors. There are 8 inputs and via 3 selection pins, the single output pin can connect to one of the inputs. In addition to 6 channels, one of the inputs is allocated for ambient noise that will be explained in detail later in its section. When the push button is pressed, a counter is increased that can be 6 at most, and 3 selection pins are adjusted according to the counter to link the correct input to the output.

The same 3 selection pins are also connected to the 7-segment display driver, CD4511B from Texas Instruments, that monitors which channel is being listened without driving the 7-segment display separately from the microcontroller. Instead of using one resistor at the common anode connection to limit the current and protect LEDs inside the display, every segment on the display has its own resistor so as to obtain the constant luminance that does not depend on the number which is shown on the display.

Despite the fact that the channel is selected via digital switch, it still has too low magnitude to be heard. Therefore, there is a headphone amplifier, LM4875, which is from Texas Instruments with features of 750 mW audio power amplifier with DC volume control and a headphone switch. The volume level can be adjusted via manual potentiometer on the device, and there is a click and pop suppression filter in the IC itself.

Besides these, there is a button for respiratory and cardiac sound filter selection that is read by the microcontroller in order to switch filters on capsule boards. In addition to this, a mechanical switch is available for future purposes that include noise cancellation studies. By using this switch, the user can listen to the unprocessed sound coming from different capsules and ambient noise reduced version of them via using the switch that will be mentioned in noise cancellation section.

3.3. Bluetooth Connectivity

Producing a wearable device that connects to a computer via USB cable is cheaper and easier but not practical especially for patients because they need to wear this device and there is a cable that connects them to a computer. Therefore, in order to communicate with a mobile phone and also a computer, Bluetooth connectivity is selected for controlling the device and also data transmission.

There are two Bluetooth modules on the main board in order to make a system with alternatives, one of them is Bluetooth 2.0 and the other one is Bluetooth 3.0 module. It communicates with the microcontroller via UART protocol with enabled handshaking to eliminate data loss. Its circuitry can be seen in Figure 3.9.

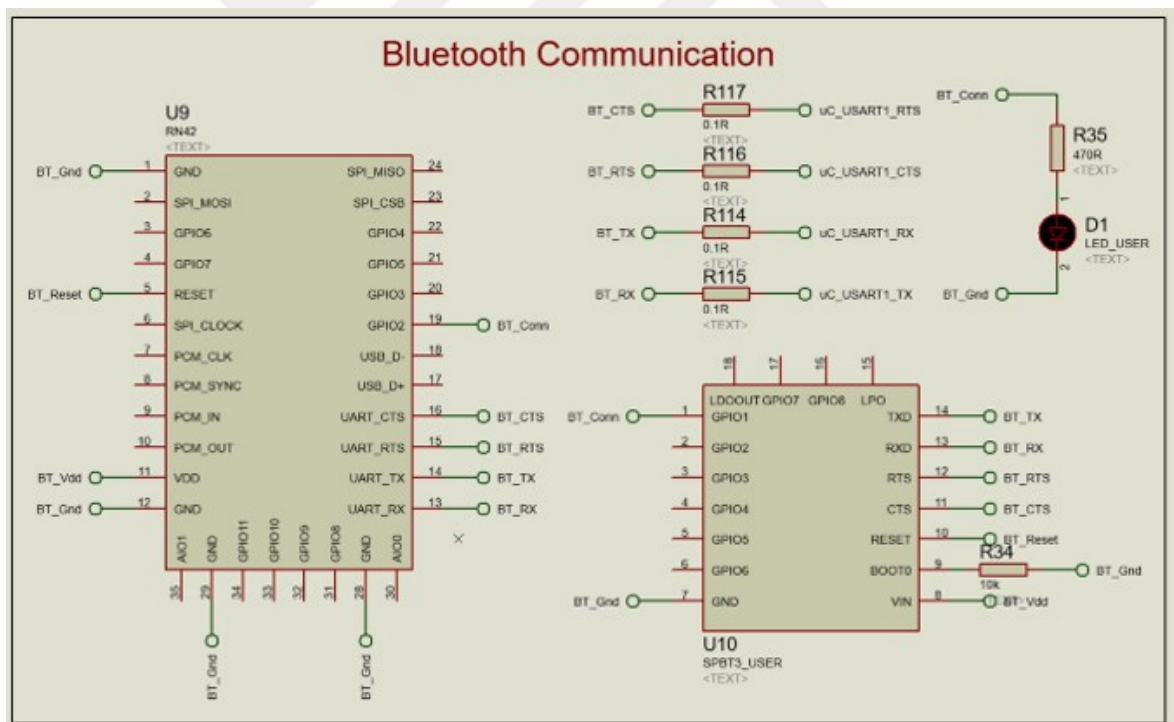


Figure 3.9. The Schematics of Bluetooth Part.

The first alternative of Bluetooth modules on the the main board is RN42 from Microchip Technology Inc. which is Class 2, Bluetooth 2.1 + EDR module, which is in operation in the instrument. There is a byte-wise communication between microcontroller and Bluetooth module through UART protocol and due to the fact that there is a continuous streaming of data to transmit acquired sounds from channels to a mobile device, RTS pin is used in order to wait while Bluetooth module is busy and to continue when it is available which is called handshaking. Without handshaking, there is loss of transmitted data because Bluetooth data transfer may not catch up with the speed of microcontroller data transmission, especially due to the increased distance between the wearable device and mobile device. In addition to handshaking precaution, a package-based data loss prevention algorithm is constructed on embedded side that will be explained throughly in embedded software chapter.

Finally, in order to obtain the fastest communication between wearable and mobile device, the baud rate of the UART communication is set as 921600 bps which is the maximum speed of this module where data and stop bits are 8 bits and 1 bit, respectively. Moreover, the password authentication is activated which is required at the beginning of pairing between devices. All of these configurations are done with AT commands via a console terminal application. There is also a special measure while drawing the Bluetooth module on PCB that is about the placement of antenna. All copper planes around Bluetooth antenna are erased according to the definition in the datasheet of RN42 [11].

Along with these aspects of Bluetooth connectivity of the main board, there is also another way in order to communicate with outside for the wearable device, USB cable connection, which is advantageous during the debugging process. Its circuit diagram can be seen in Figure 3.10.

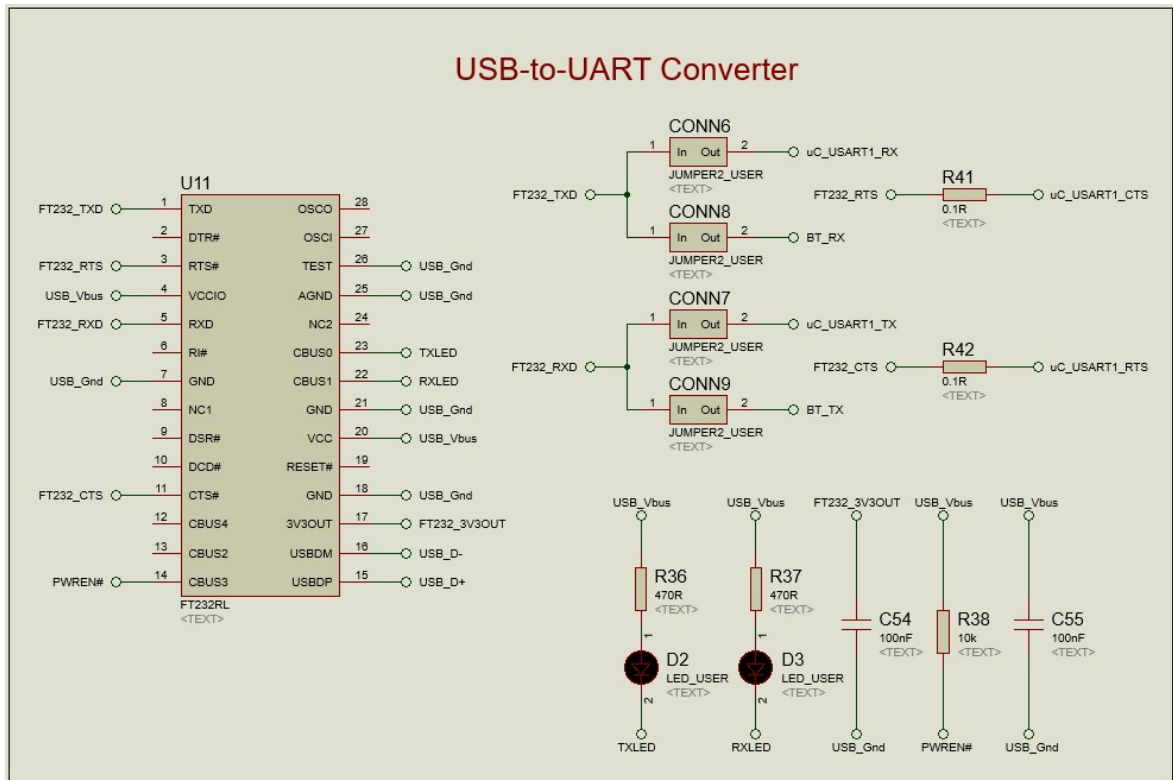


Figure 3.10. The Schematics of USB Connection Part.

FT232 from FTDI Chip, is the most generic and commonly used USB-to-UART converter IC in many electronics devices. Through this and 4 jumper connectors that can be seen in 3.10., not only can the data can be transferred from wearable device to computer, but also Bluetooth module via AT commands can be programmed if jumpers are placed at the predefined positions. Two LEDs indicate whether TX or RX pins are active or not.

3.4. Memory

Because of the fact that the wearable device can reach up to 6 channels, and there are additional sensors such as pneumotachograph, stretch sensor, accelerometer and pulse oximeter, there is a necessity for larger memory space. In order to meet this requirement, there are several memory options that can be divided into two groups, one of them is IC memories that are serial and parallel memory ICs and the other one is microSD Card.

3.4.1. IC Memories

There are two types of IC memories on the main board, the first one is parallel memory IC, IS62WV10248 from Integrated Silicon Solution Inc., that has a capacity of 8 Mb that is enough to store up to 8 channels or 4 channels with respiratory and heart sounds together. Reading and writing processes of parallel memories are very fast such that their access time is 45 ns due to the fact that there is no sequential data transmission and that it has 20-bit address and 8-bit data ports, so a single byte can be written or read in one cycle while it would take at least 28 cycles in serial memory. In spite of the speed advantage, parallel memories have larger footprints and also consume more GPIO pins on microcontrollers. Its schematic can be found in Figure 3.11.

Another IC memory option is the serial one, that is S25FL128S from Cypress Semiconductor. It does have a QSPI communication interface which is 4 times faster than SPI interface so is called as QSPI. It has a capacity of 128 Mb and a small footprint, however it is slower than the former option. Its schematics can be seen in Figure 3.12.

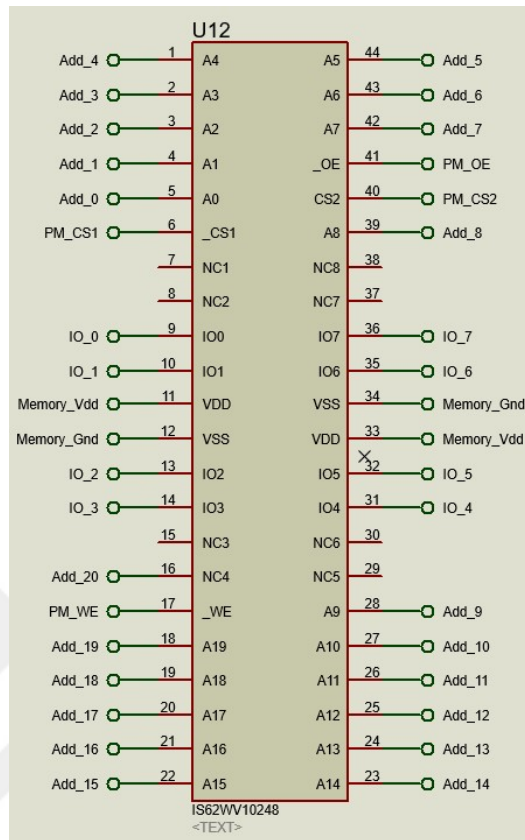


Figure 3.11. The Schematics of Parallel Memory Part.

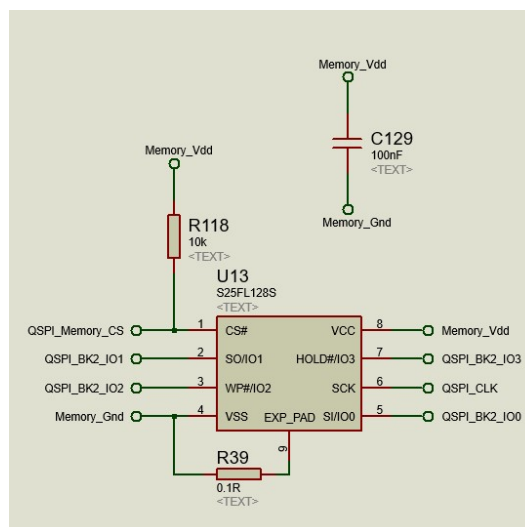


Figure 3.12. The Schematics of Serial Memory Part.

3.5. Other Features

3.5.1. Power Management

There is a Lithium-Polymer battery on the main board that powers the circuit. It is a rechargeable battery via USB connection that gives 5 V but it should be reduced to 4.2 V to charge the battery. Then, a single cell, Li-Ion/Li-Polymer charge management controller, MCP73812 from Microchip Technology Inc. is used. This converts the incoming 5 V to 4.2 V that is the highest allowable voltage in order to charge single cell batteries. By controlling charger enable pin with microcontroller, its charge level can be read. At the beginning of the design process, the circuit with two batteries have been thought due to the complete separation of analog and digital side, however, it was a precaution and it is not necessary anymore because it has never been observed that they interfere each other.

For the USB side, there is a ferrite bead and a capacitor in order to protect the circuit against voltage surges while USB cable is plugged in and out. There are also two resettable fuses in order to protect the circuit against excessive current coming from USB cable. In the case of excessive current, they interrupt the current flow and guard the circuit, and return back their normal position if the current is reduced below maximum allowable current rate. Their schematic can be seen in Figure 3.14.

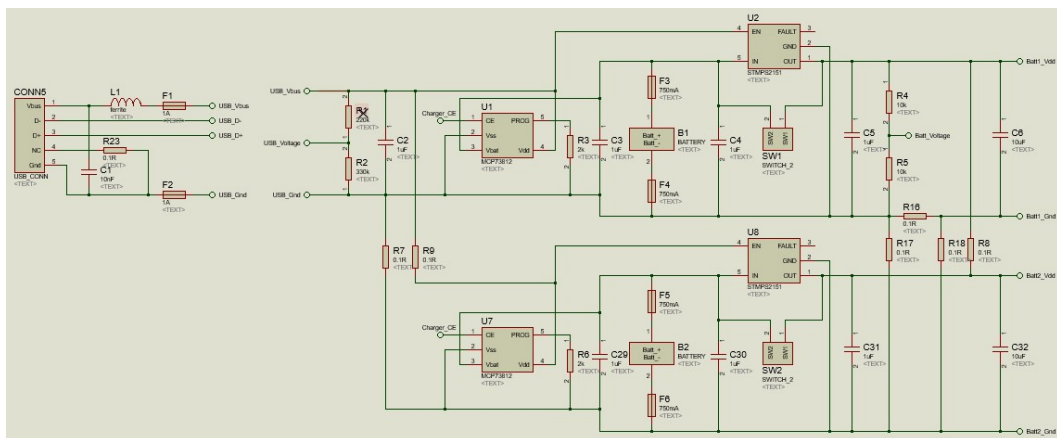


Figure 3.14. The Schematics of Power Management Part.

Power distribution is also designed carefully that separates digital and analog power lines. TPS73633 from Texas Instruments is selected because of the fact that it is a low-dropout voltage regulator, and also does have low noise and high PSRR features. Its circuitry can be seen in Figure 3.15.

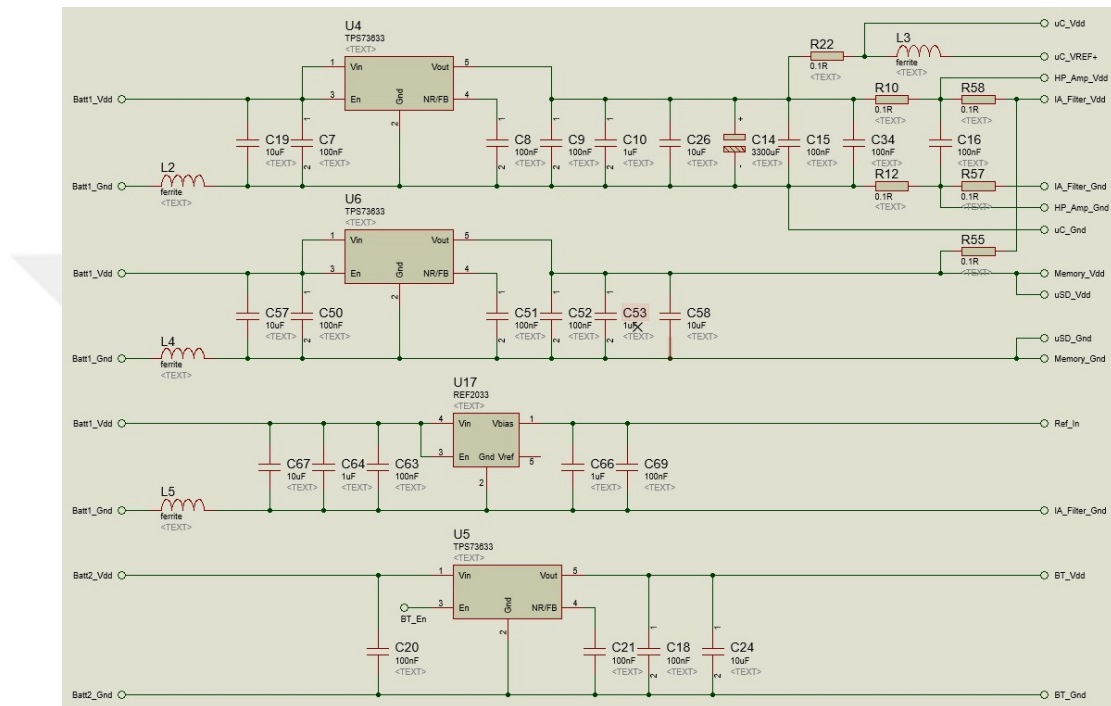


Figure 3.15. The Schematics of Power Distribution Part.

3.5.2. Stretch Sensor

It is required to synchronize respiratory sounds with respiratory flow phase in order to reach better diagnosis results. Therefore, because it is a wearable device, a resistive stretch sensor is implemented inside the corset that expands during inspiration and shrinks during expiration. The stretch sensor is depicted in Figure 3.16.

In order to measure the resistance of a sensor, there is a basic voltage divider and a voltage follower circuit for preprocessing purposes before ADC reading on the microcontroller. Its circuitry can be found in Figure 3.20.



Figure 3.16. The Resistive Stretch Sensor [12].

3.5.3. Pneumotachograph and Pulse Oximeter

A pneumotachograph can be connected to the main board via RCA connector as mentioned in the Introduction chapter. There is a ground connection and also 1.65 V reference voltage supply on the RCA connector, that comes from REF2033, a precise voltage reference IC from Texas Instruments. The respiratory flow phase signal can be sampled and quantized via ADC on the microcontroller through RCA connector. The connector is depicted in Figure 3.17

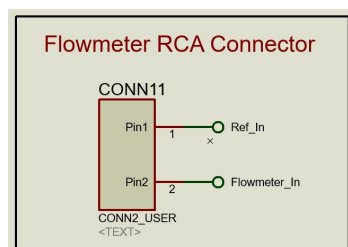


Figure 3.17. The Connector of Pneumotachograph.

For future studies, a pulse oximeter interface and connector are available for MAX30100 from Maxim Integrated which is a compact and cheap pulse oximeter sensor in a single package. Its working principle and I2C interface circuitry can be seen in

Figure 3.18 and Figure 3.19, respectively.

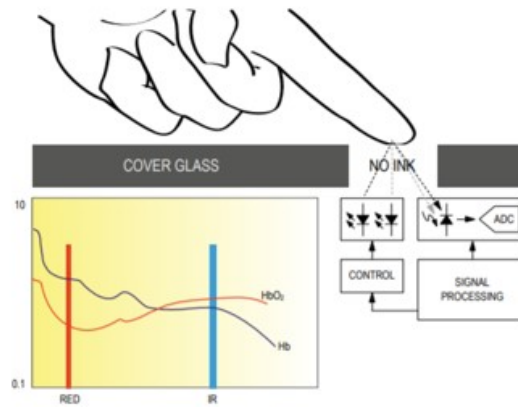


Figure 3.18. The Working Scheme of Pulse Oximeter [13].

3.5.4. Ambient Noise Cancellation

Noise cancellation is also implemented for future purposes that is intended by adding an ambient noise microphone on the main board to extract ambient noise from respiratory and heart sounds for better sound quality and accurate diagnosis. The same circuitry in each capsule boards is drawn on the main board for noise cancellation in order to equalize the phase difference and frequency response between the exact and ambient microphones. Through this, both signals travel approximately the same route while passing through the instrumentation amplifier and the band pass filter, and the phase difference between them is reduced. Also, for respiratory and heart sound filters, the ambient noise input is also filtered according to the filter selection. It is a trial circuitry and can be used in future studies and is depicted in Figure 3.20.

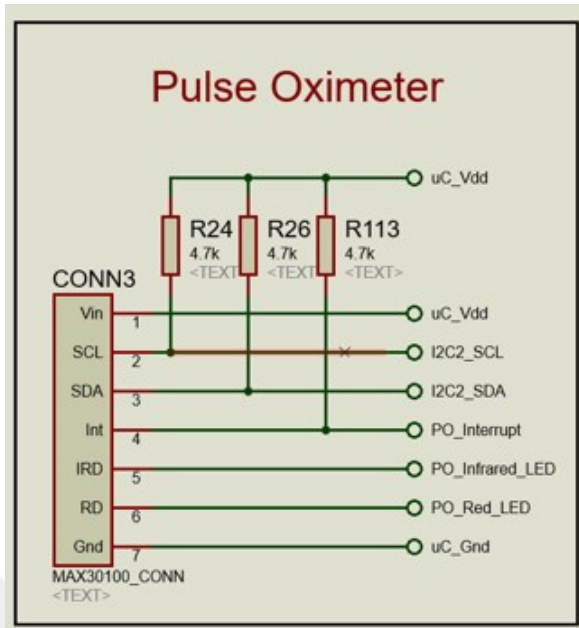


Figure 3.19. The I2C Interface of Pulse Oximeter.

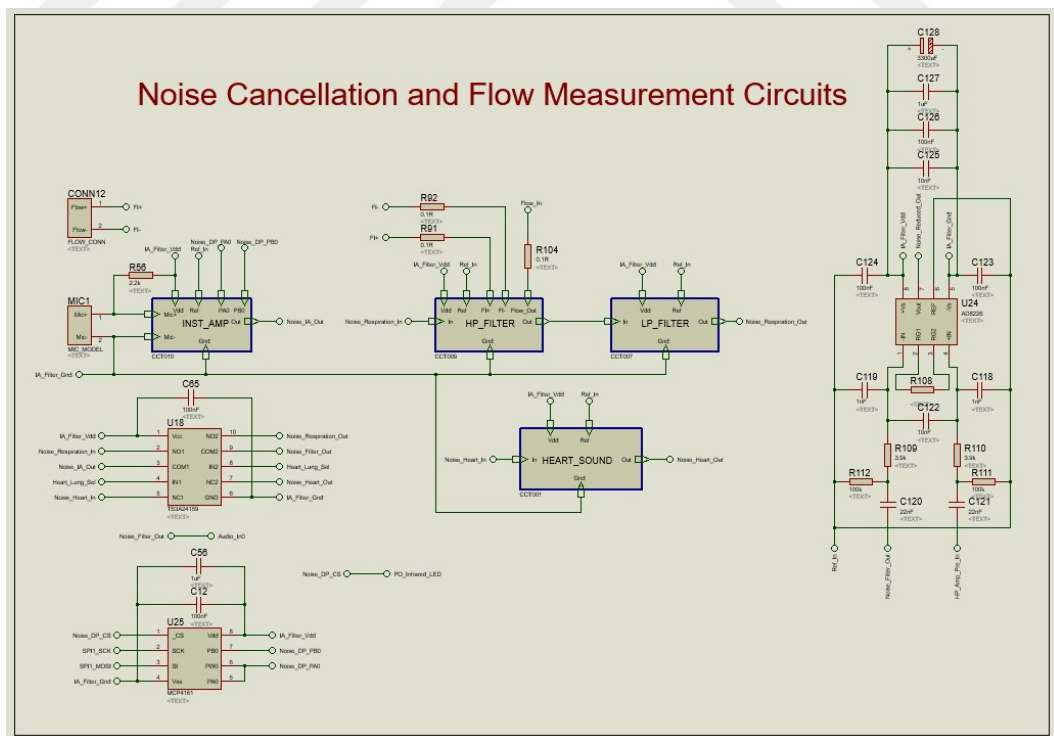


Figure 3.20. The Schematics of Ambient Noise Cancellation and Respiratory Flow Phase Detection Circuit.

4. CAPSULE BOARD

The capsule board is the second PCB board of the system and its general architecture can be seen in Figure 4.1.

Briefly, there are two microphones at the input stage of the circuit, the first one is the main microphone for auscultation, however, the second one is for noise cancellation for future purposes. The main idea is taking the advantage of CMRR of instrumentation amplifier that is actually a noise cancellation mechanism. Nevertheless, this has not been implemented yet on the circuit. When microphone 2 is short-circuited, the circuit continues its normal operation without noise cancellation feature.

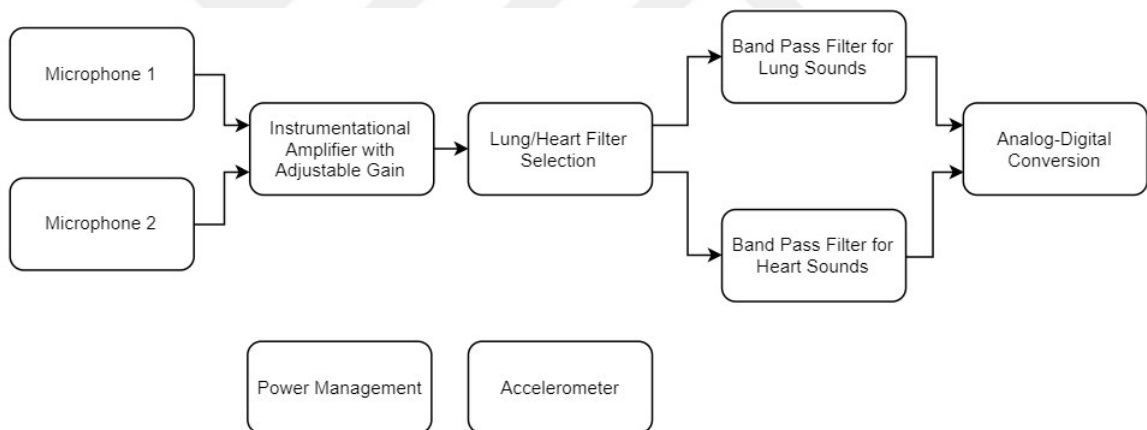


Figure 4.1. The General Architecture of the Capsule Board.

There is an instrumentation amplifier which has a gain adjustment capability thanks to a digital potentiometer. The volume level of the auscultation can be increased and decreased according to the body size, age and sex of patients.

After the amplification, the signal passes through two switches and one BP filter that can be selected as lung or heart sounds filter. Then, an ADC converts the analog signal into digital one and transmits to the main board via SPI protocol.

Additionally, there is a power management part that includes a voltage regulator and a voltage reference, and also an accelerometer for future studies that can give us valuable information about the respiratory flow phase.

Its layout drawing and PCB products can be seen in Figure 4.2 and Figure 4.3, respectively.

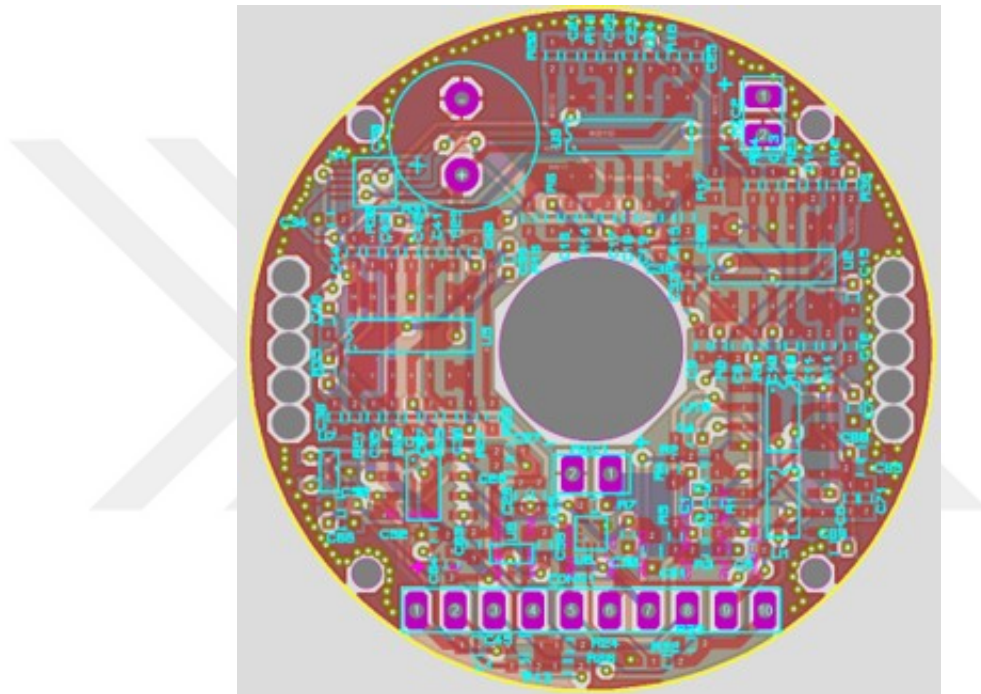


Figure 4.2. The Layout of the Capsule Board.

The PCBs are also 4-layer and gold immersed in order to create Faraday Cage protection mechanism which is especially crucial for analog circuits. The final productions of the capsule boards including microphone and its own capsule placed on it can be seen in Figure 4.4.

In Figure 4.5 and Figure 4.6, the final products of the system that combines its textile, main and capsule boards can be seen. The technical drawing of the microphone capsules can be seen in Appendix A.

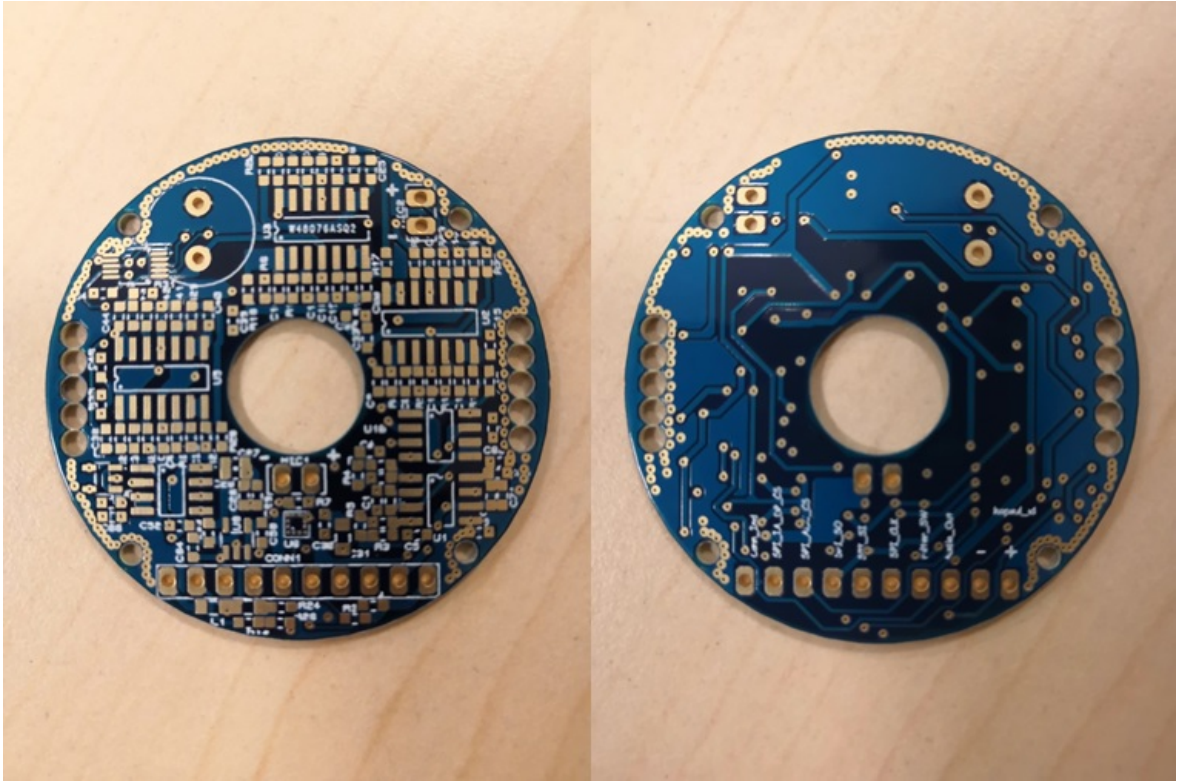


Figure 4.3. The PCB Products of the Capsule Board.

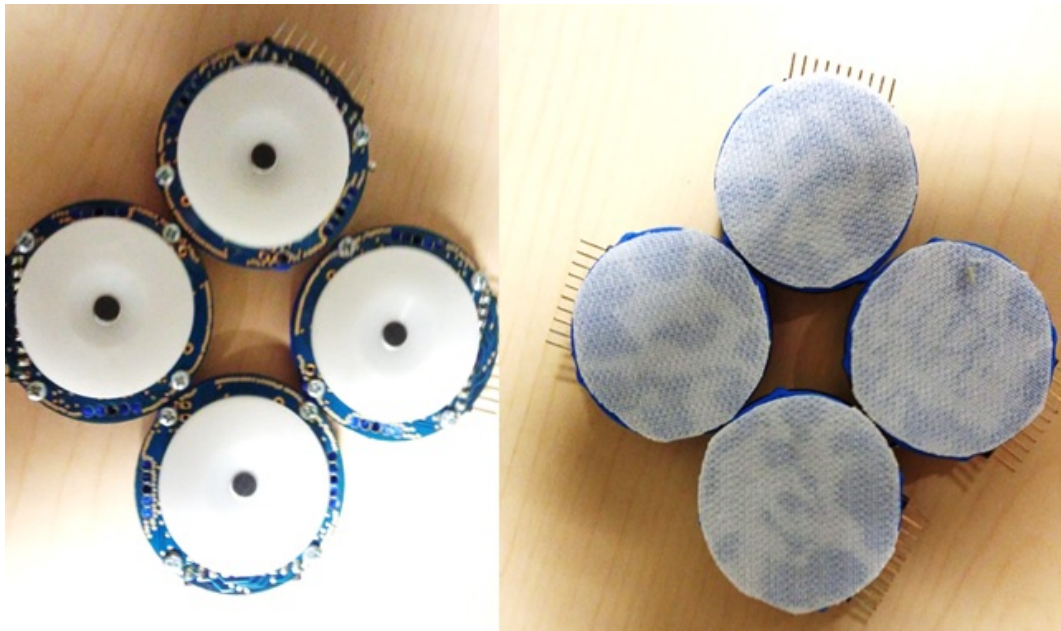


Figure 4.4. The Final Products of the Capsule Boards.

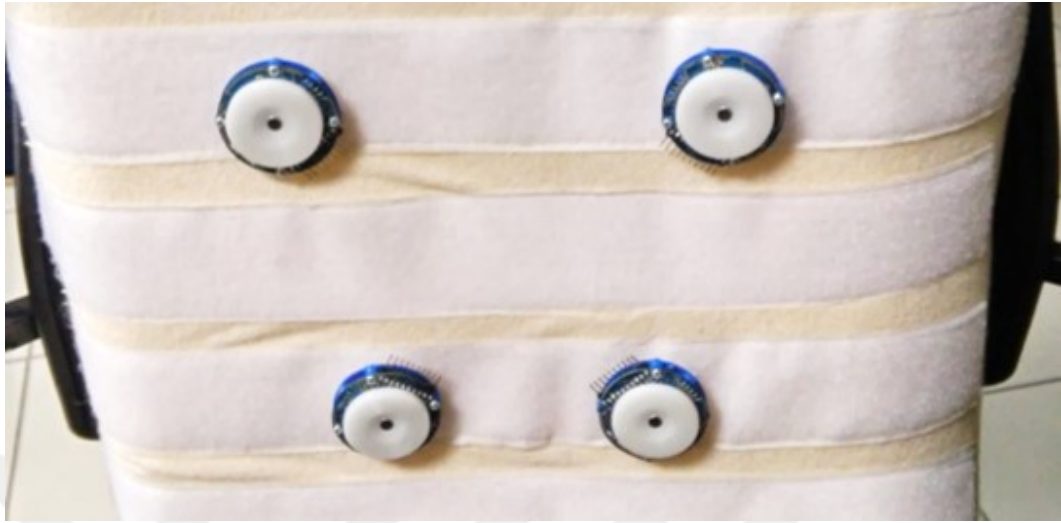


Figure 4.5. The Final Product of the Wearable Device with Pillow Option.

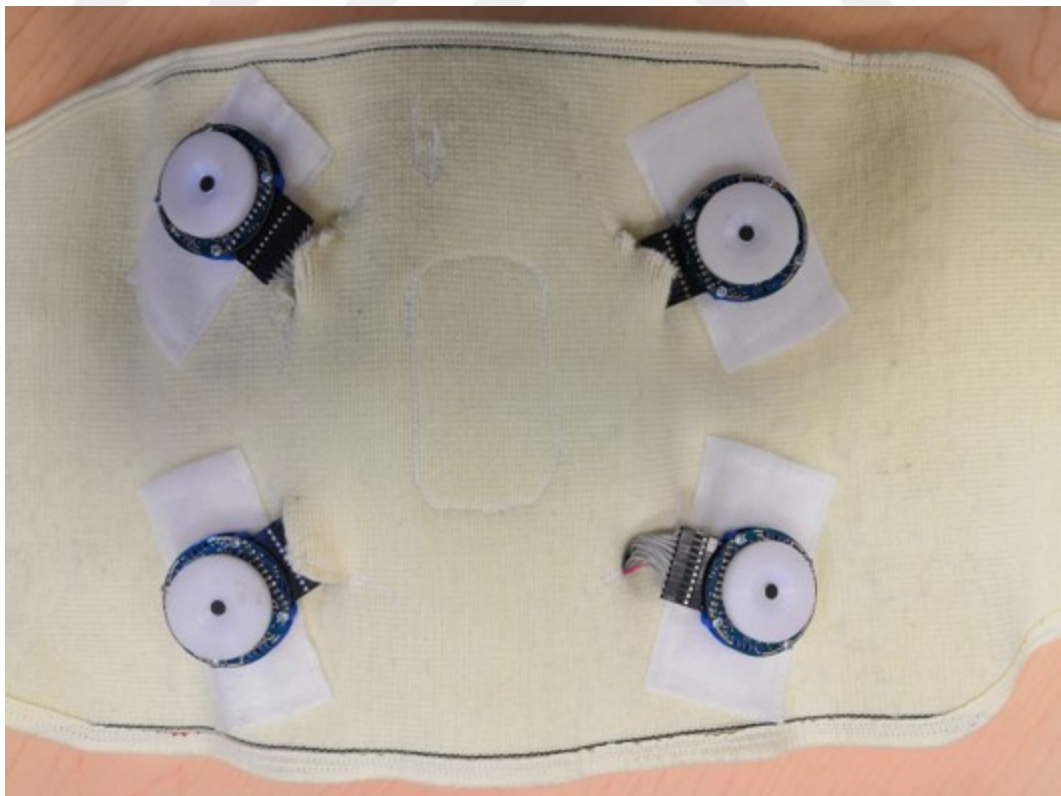


Figure 4.6. The Final Product of the Wearable Device with Corset Option.

There is a 10-pin connector on each capsule board in order to connect with the main board, which includes SPI interface for ADC and digital potentiometer, I2C interface for accelerometer, audio signal, battery voltage, and filter selection and connection indication pins.

As a multi channel device including a main board and its slaves, there were two power distribution options at the design stage, one of them is using a single voltage regulator and a voltage reference, that is crucial especially for the instrumentation amplifier and BP filters, on the main board, and all capsule circuits can be supplied from the same regulator and the reference IC. Another option is that supplying the battery voltage to all capsule circuits in order to allow them to convert their required voltages and references themselves. Both of the alternatives for power distribution scheme can be seen in Figure 4.7 and Figure 4.8.

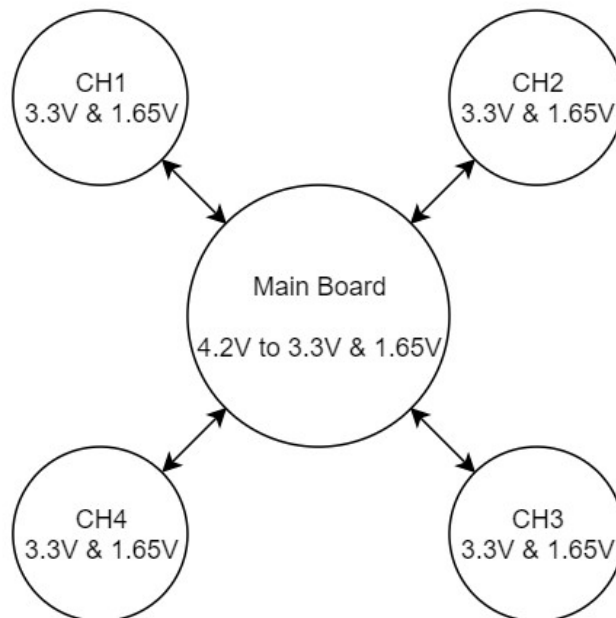


Figure 4.7. The Block Diagram of General Supply and Reference Voltages Generation Scheme.

The advantage of the general voltage generation scheme is that there is only one voltage regulator placed on the main board instead of using that ones as much as the number of capsule boards used. Since each capsule board consumes approximately 20

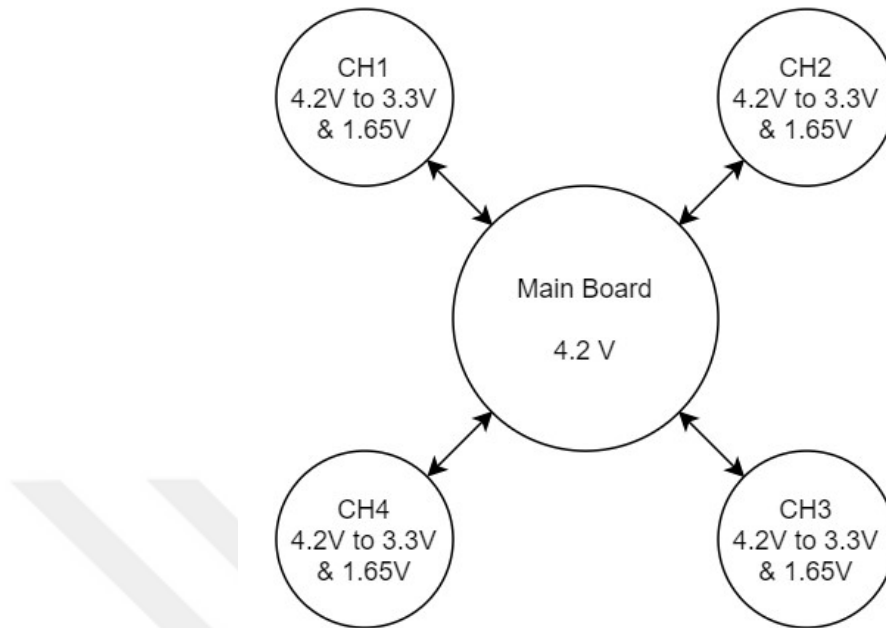


Figure 4.8. The Block Diagram of Local Supply and Reference Voltages Generation Scheme.

mA while it is operating, it is sufficient to use the same voltage regulator IC on the main board to supply all 6 channels. This is also valid for voltage reference generation that is required on analog signal preprocessing circuits to oscillate the incoming signal around 1.65 V instead of 0 V.

However, despite being a cheaper solution, the fact that reference voltage signals should travel between main and capsule boards that makes it vulnerable to interference from outside. Moreover, if the reference voltage is not clean, the acquired lung and heart sounds are distorted.

As a result, although being more expensive, the latter alternative is more preferable with respect to the former one. The main reason behind this is that every supply and reference voltages will be generated on their own PCBs and the number of voltage regulators and voltage reference ICs used will be as many as how many capsule boards are used, however, each supply and reference voltage lines will become as short as pos-

sible and undisturbed. This is a major advantage over the previous option. Therefore, the second power distribution scheme is selected for better signal quality.

The general schematics of one capsule board can be seen in Figure 4.9.

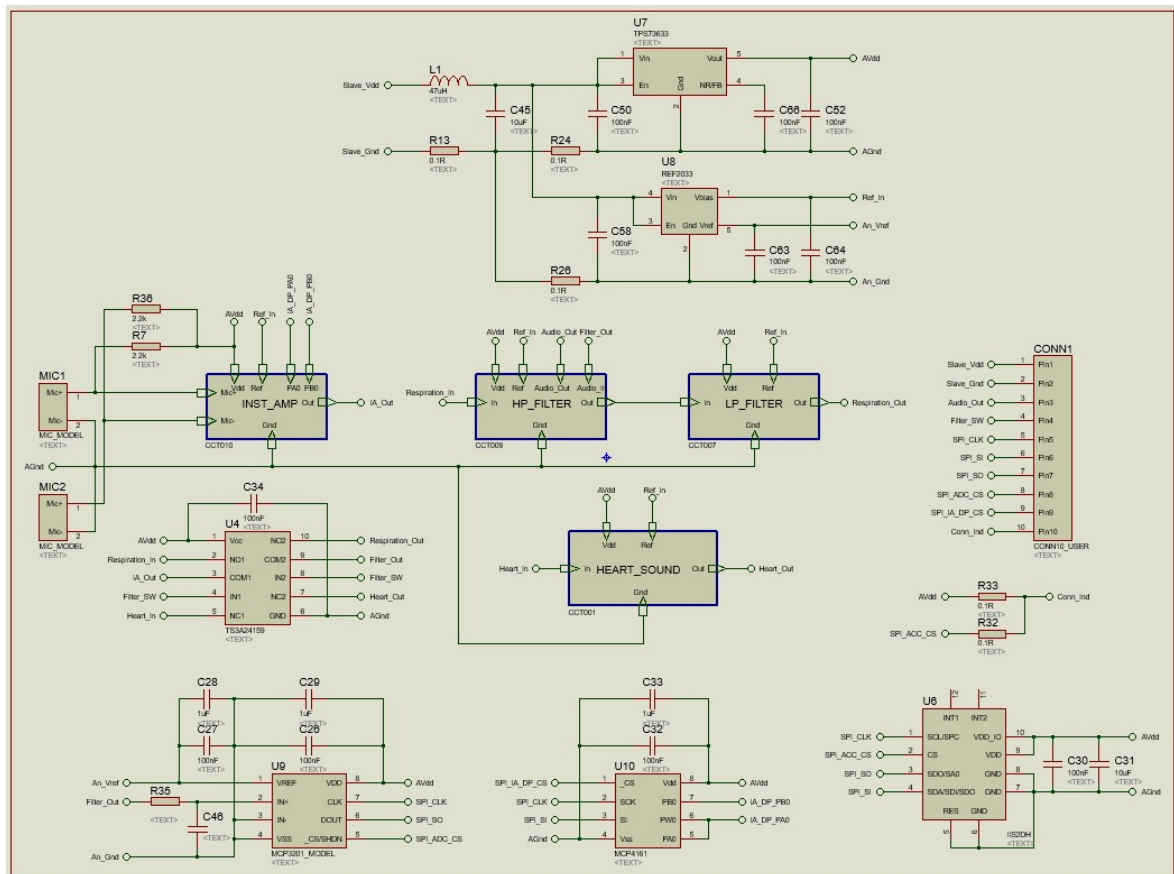


Figure 4.9. The Schematics of Capsule Board.

4.1. Instrumentation Amplifier

An electret microphone is used for auscultation in the capsule board that is placed in a special capsule that is explained later in the text. The microphone is POM-2245L-C33R from PUI Audio that has the sensitivity of -45 dB. Its datasheet is shown in Appendix C [18]. Because electret microphones have lower magnitude, they need to be amplified via an instrumentation amplifier, which is AD8226 from Analog Devices. Its circuitry is shown in Figure 4.10.

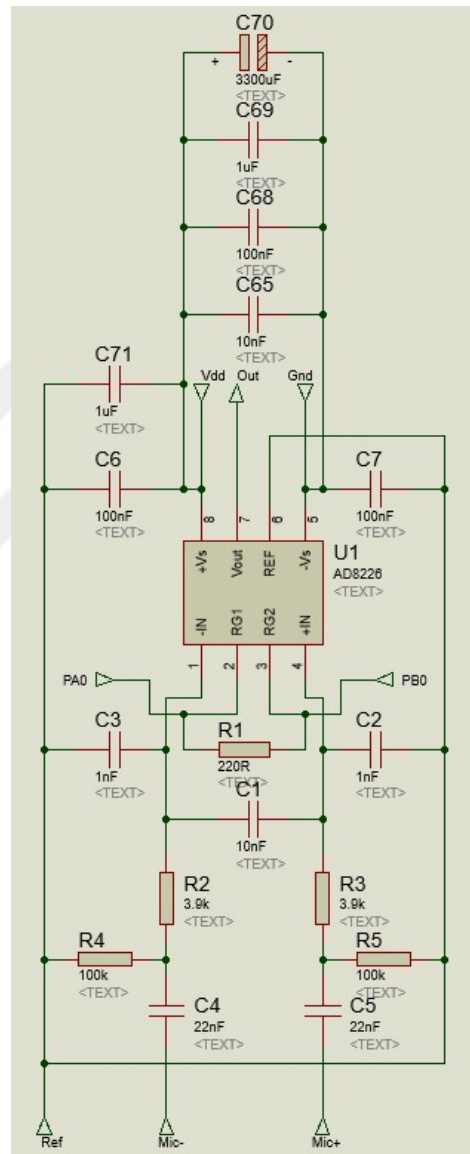


Figure 4.10. The Schematics of Instrumentation Amplifier.

Its gain is calculated according to Equation 4.1 where R_g is the resistor connected across 2nd and 3rd pins of the instrumentation amplifier,

$$Gain = 1 + \frac{49.4k\Omega}{R_g} \quad (4.1)$$

There is an RFI suppression stage with a low-pass RC network at the input of the circuit in order not to amplify incoming noise from outside. Moreover, a digital potentiometer is added parallel to the pins of the resistor that adjusts the gain of the amplifier. Therefore, if the gain resistor is not soldered, the gain level of the instrumentation amplifier can be controlled digitally. In addition to these, there are several decoupling capacitors with different sizes in order to stabilize supply and reference voltages against fast and slow transients.

A digital potentiometer used in the circuit which is MCP4161 from Microchip Technology Inc., that uses SPI protocol to receive command from the microcontroller and changes the resistance between its output pins. The resistance value can be controlled up to 10 k Ω with 257 intermediate steps. Its schematic on the capsule board can be seen in Figure 4.11.

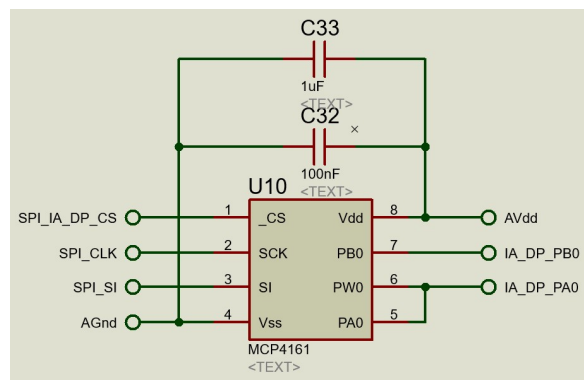


Figure 4.11. The Schematics of Digital Potentiometer.

4.2. Pulmonary Sound Filter

There are two types of filters on each capsule circuit, and the first one is pulmonary sound filter. It is a band pass filter and designed as cascaded 6th order Bessel HP and 8th order Butterworth LP filters that are constructed in Sallen-Key topology. Instead of using Tow-Thomas topology which requires more OPAMPS so as to build a 2nd order filter with respect to Sallen-Key do, Sallen-Key topology is used for both filters. However, the main disadvantage of Sallen-Key topology against Tow-Thomas is that Sallen-Key topology is more sensitive to component variations. In order to solve this problem, all resistors and capacitors are purchased with 1% and 5% tolerances, respectively.

4.2.1. High-Pass Filter

This is a 6th order Bessel high-pass filter with 80 Hz cutoff in order to limit the incoming signal below 80 Hz and also linear phase response [7]. Its circuit diagram can be seen in Figure 4.12.

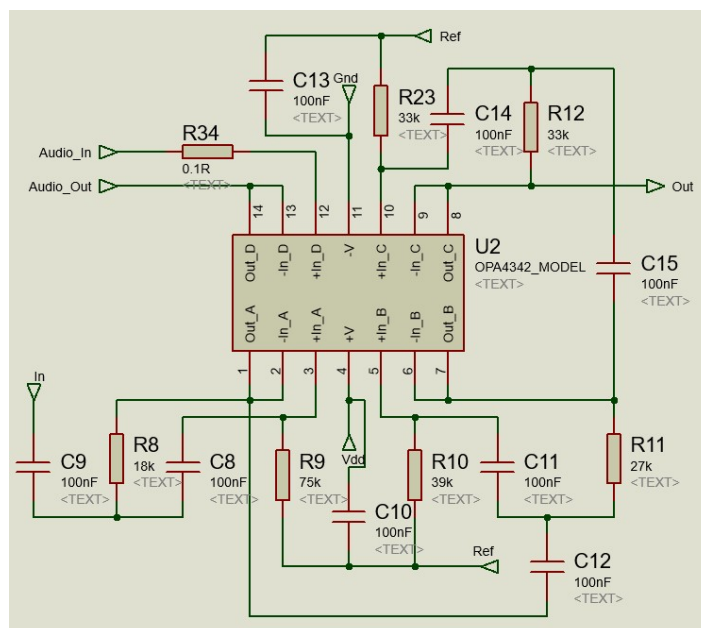


Figure 4.12. The Schematics of High Pass Filter for Pulmonary Sound.

As OPAMP, OPA4342 from Texas Instruments is used that includes 4 OPAMP inside one package. For 6th order high-pass filter with Sallen-Key topology, 3 OPAMPs are enough so the last OPAMP is used for voltage follower to isolate audio signal on headphone apart from the disturbance of ADC sampling process.

The circuit diagram of a typical Sallen-Key or KRC topology for high-pass filter can be seen in Figure 4.13.

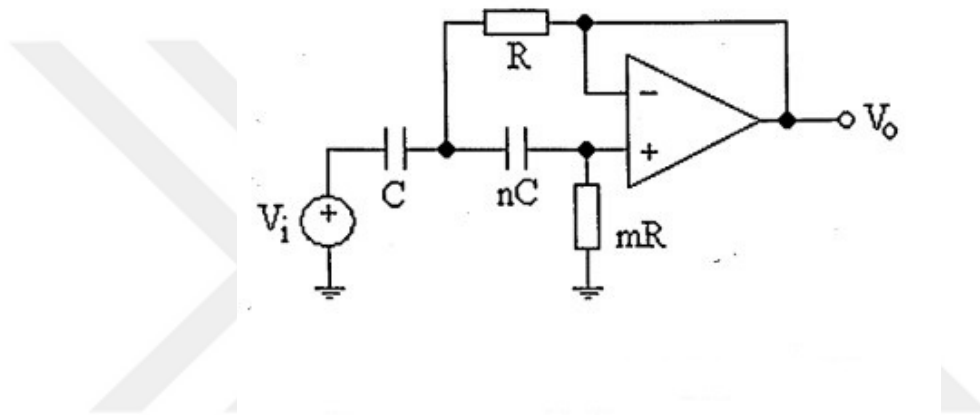


Figure 4.13. The Circuit Diagram of Sallen Key Topology for High Pass Filter [14].

Design equations of the second order KRC filter are

$$f_0 = \frac{1}{2\pi RC\sqrt{mn}} \quad (4.2)$$

$$Q = \frac{\sqrt{mn}}{n+1} \quad (4.3)$$

According to the values on the Table 4.1, the stages of 6th order Bessel filter are cascaded from high to low Q in order to reduce noise. Therefore, the cutoff frequencies of each stage are described in Table 4.2 with the Equation 4.4.

Table 4.1. Bessel Filter Table for 6th Order Filter Design [15].

	1st f_{0table}	1st Q	2nd f_{0table}	2nd Q	3rd f_{0table}	3rd Q
Value	1.606	0.510	1.691	0.611	1.907	1.023

$$f_0 = \frac{f_c}{f_{0table}} \quad (4.4)$$

Table 4.2. Cutoff Frequency Table for 6th Order Bessel Filter Design [15].

	f_0 (Hz)	Q
Stage 1	41.95	1.023
Stage 2	47.039	0.611
Stage 3	49.813	0.510

By taking into account the availability of passive components on the market, in order to satisfy the requirements in Table 4.2, resistor and capacitor values of each stage are calculated and can be found in Table 4.3.

Table 4.3. Component Values for 6th Order Bessel Filter Design.

	R (Ω)	mR (Ω)	C (F)	nC (F)
Stage 1	18k	75k	100n	100n
Stage 2	27k	39k	100n	100n
Stage 3	33k	33k	100n	100n

4.2.2. Low-Pass Filter

This is an 8th order Butterworth low-pass filter with 2000 kHz cutoff frequency in order to limit the incoming signal beyond 2000 Hz [7]. Its circuit diagram can be seen in Figure 4.14.

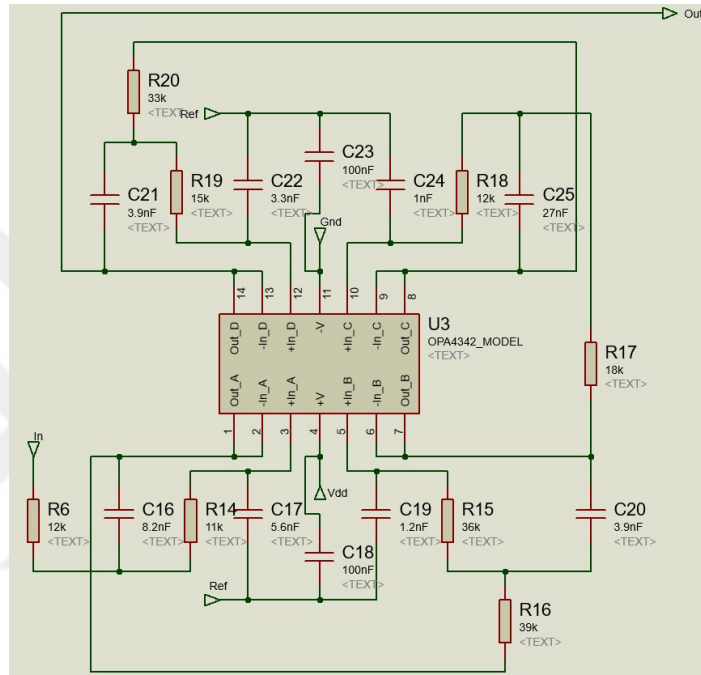


Figure 4.14. The Schematics of Low Pass Filter for Pulmonary Sound.

The circuit diagram of a typical Sallen-Key or KRC topology for low-pass filter can be seen in Figure 4.15.

Design equations of the second order KRC filter are

$$K = 1 + \frac{R_B}{R_A} \quad (4.5)$$

$$f_0 = \frac{1}{2\pi RC\sqrt{mn}} \quad (4.6)$$

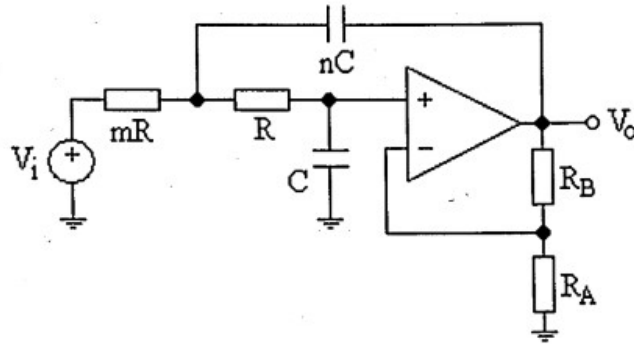


Figure 4.15. The Circuit Diagram of Sallen Key Topology for Low Pass Filter [14].

$$Q = \frac{\sqrt{mn}}{(1 - K)m + m + 1} \quad (4.7)$$

Table 4.4. Butterworth Filter Table for 8th Order Filter Design [15].

	$f_0(Hz)$	1st Q	2nd Q	3rd Q	4th Q
Value	2000	0.5098	0.6013	0.900	2.5628

According to the values on the Table 4.4, the stages of 8th order Butterworth filter are cascaded from high to low Q in order to reduce noise. By taking into account the availability of passive components on the market, in order to satisfy the requirements in Table 4.4, resistor and capacitor values of each stage are calculated and can be found in Table 4.5.

The frequency response of the band pass filter for pulmonary sound can be seen in Figure 4.16.

Table 4.5. Component Values for 8th Order Butterworth Filter Design.

	\mathbf{R} (Ω)	\mathbf{mR} (Ω)	\mathbf{C} (F)	\mathbf{nC} (F)
Stage 1	11k	12k	5.6n	8.2n
Stage 2	36k	39k	1.2n	3.9n
Stage 3	12k	18k	1n	27n
Stage 3	15k	33k	3.3n	3.9n

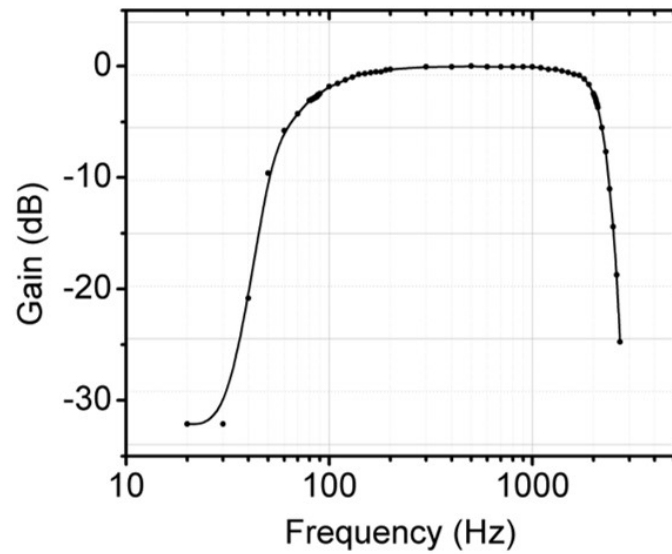


Figure 4.16. The Frequency Response of the Band Pass Filter for Pulmonary Sound.

Table 4.6. Butterworth Filter Table for 4th Order Filter Design [15].

	$f_0(Hz)$	1st Q	2nd Q
Value	30 and 500	0.5412	1.3065

Table 4.7. Component Values for 4th Order Butterworth High Pass Filter Design.

	R (Ω)	mR (Ω)	C (F)	nC (F)
Stage 1	51k	56k	100n	100n
Stage 2	20k	130k	100n	100n

Table 4.8. Component Values for 4th Order Butterworth Low Pass Filter Design.

	R (Ω)	mR (Ω)	C (F)	nC (F)
Stage 1	24k	62k	6.8n	10n
Stage 2	5.6k	18k	10n	100n

The frequency response of the band pass filter for cardiac sound can be seen in Figure 4.18.

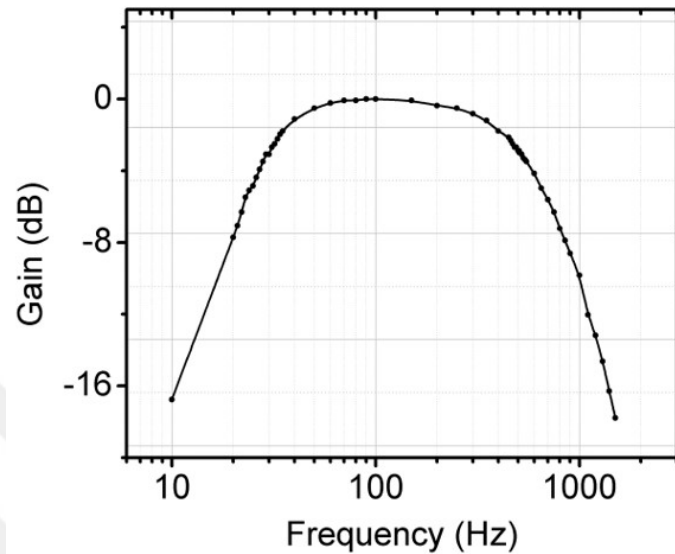


Figure 4.18. The Frequency Response of the Band Pass Filter for Cardiac Sound.

4.4. Analog-to-Digital Conversion

MCP3201 from Microchip Technology Inc., which is a 12-bit ADC IC is used on each capsule circuit in order to convert analog signals into digital ones. Although 10-bit resolution is enough for our purposes, 12-bit ADC is selected in order to improve ADC accuracy. Two LSB bits of each sample are removed so as to acquire samples with exact 10-bit resolution.

There is a basic, RC low pass filter at the input stage of ADC in order to suppress undesired signals. Also, various decoupling capacitors with different values that are placed near the ADC protect supply and reference voltages against transients. Its schematics can be seen in Figure 4.19.

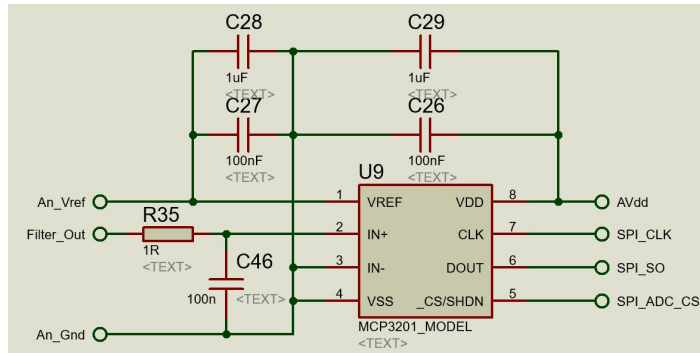


Figure 4.19. The Schematics of Analog to Digital Converter IC.

4.5. Other Features

4.5.1. Power Management

The same ICs for power management used on the main board, are also used on each capsule circuit. Its schematic can be seen in Figure 4.20.

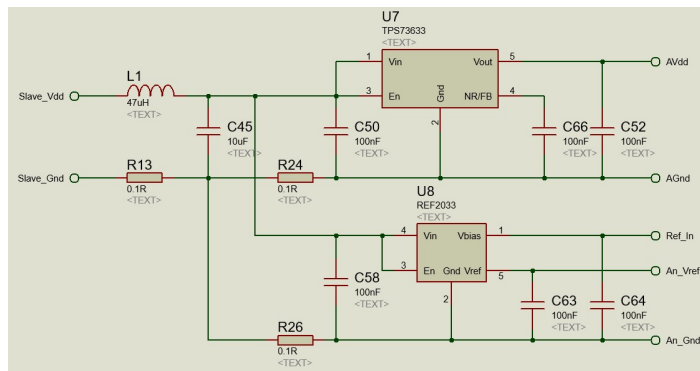


Figure 4.20. The Schematics of Power Management on Capsule Board.

4.5.2. Accelerometer

Because of the fact that it is a wearable device, the main board is placed on the center, and each capsule board is placed on the predefined region on the back side of the chest. Moreover, while the patient is inspiring and expiring, each capsule board can move together due to the expanding and narrowing of the circumference of the chest. Therefore, for future purposes, an accelerometer on each capsule board may be useful for understanding the phase of the respiratory flow via chest movements. IIS2DH from ST Microelectronics is used and its circuit diagram can be shown in Figure 4.21.

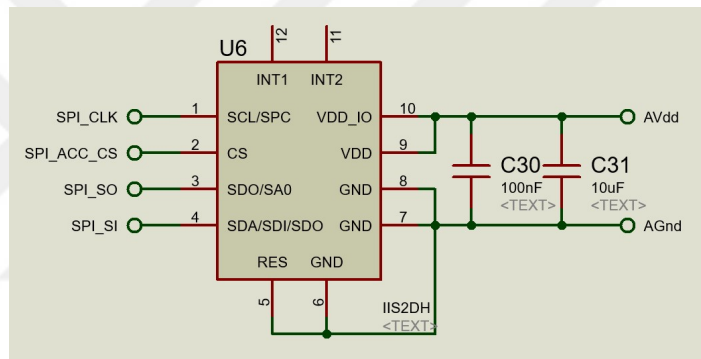


Figure 4.21. The Schematics of Accelerometer.

5. EMBEDDED SOFTWARE

Due to the fact that it is a wearable and battery powered, portable device, there is a necessity for a microcontroller in order to communicate with peripherals and to process signals. Therefore, STM32F777 from ST Microelectronics is used on the main board, and also there is an embedded software which runs on the microcontroller to fulfill its tasks.

The embedded code is written using HAL library from ST Microelectronics that makes the process of initialization at the design stage and also migration from one microcontroller to another one, easier.

The main flow diagram of the embedded code can be seen in Figure 5.1.

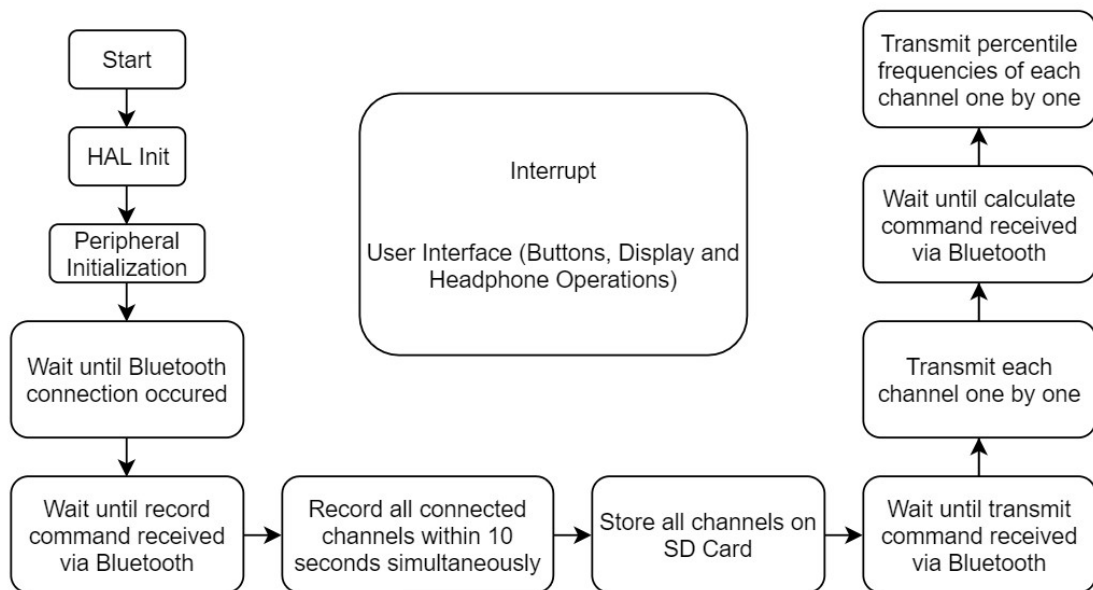


Figure 5.1. The Main Flow Diagram of the Embedded Code.

In order to interpret the operation scheme of the main code, it starts with HAL initialization. After this, peripherals of the microcontroller, which are GPIO, SPI, SD-MMC, ADC, TIM and UART are configured that means all peripherals are assigned according to their tasks, and their parameters are defined. Throughout all stages on the flow diagram, channels can be auscultated via headphone jack without any extra operations or command. Bluetooth connectivity and record command from mobile device or console application are required to start record session of all channels simultaneously.

Each channel samples are collected at the same time with 9600 samples/second rate, that corresponds to sampling each channel approximately at every 104 microseconds.

Because of the fact that 10-bit ADC sampling is used, and microcontrollers are based on bytes with 8-bits, 4 samples are stored as 5 bytes on the memory region. While writing and reading processes of these bytes, there is a coder and an encoder functions for memory operations on the embedded code.

After each channel is captured, they are stored on the SD Card and device starts to wait transmission command from the mobile or console application. Then, from channel 1 to the last channel, captured samples are transmitted with lossless transmission mechanism that can be seen in Table 5.1.

Table 5.1. The Package Mechanism of Data Transmission.

1 byte	1250 bytes	2 bytes
Package Number	Auscultation (1000 samples)	Phase of Respiration (1 sample)

A timer which is called TIM3 on the embedded code is used for periodic sampling. It is configured in order to trigger an interrupt at every 104 microsecond to sample each channel at the same time. After record session is completed, it is disabled.

In the case of 10 seconds record session and 9600 samples/second sampling rate, each channel creates 96000 samples and 960000 bits due to 10-bit sampling and 120 kByte at the end of each recording. During data transmission process, first the package number is sent. Then, 1250 bytes for 1000 samples are transmitted and the package is ended with the phase of respiratory flow sample. The number of bytes of each package is 1253 byte, and if one of the is missing, it is easy to understand on the other side of the communication, on mobile device or console application. Therefore, the only missing package can be demanded from the wearable device with a command easily.

The last command is about percentile frequency calculation for each channel that is performed on the embedded side, and its results also delivered to mobile device or console application. Percentile frequency calculation is described in detail in Chapter 6.

6. PERCENTILE CALCULATION ALGORITHM

While one of the two main objectives of the system is data acquisition, the other one is basic signal processing on the embedded side.

Instead of using high level libraries, percentile frequencies of each channel are calculated with low level functions for efficiency and accuracy. Previously, high level libraries have been tried, however, when they are compared with the results of MATLAB on the same signals, they were not accurate as MATLAB results. Therefore, low level functions have been used to calculate percentile frequencies that can be found in Appendix B [16].

While calculating the PSD of the system, FFT with 256 samples with Hamming window and 50% overlap is used in order to calculate the PSD of each window [17].

Because of the fact that there are two inspiration and two expiration sections in our records, exhale sections are used for percentile frequency calculation because they are louder than the other ones, and also their average is calculated so as to create one result for each channel.

Percentile frequencies are the frequencies that are the boundaries between 25%, 50%, 75% and 90% regions of the power spectral density of the signal that can be seen in Figure 6.1. The advantage of finding percentile frequencies is that the percentile frequencies of respiratory sounds of unhealthy subjects tend to become higher than the percentile frequencies of healthy subjects [8].

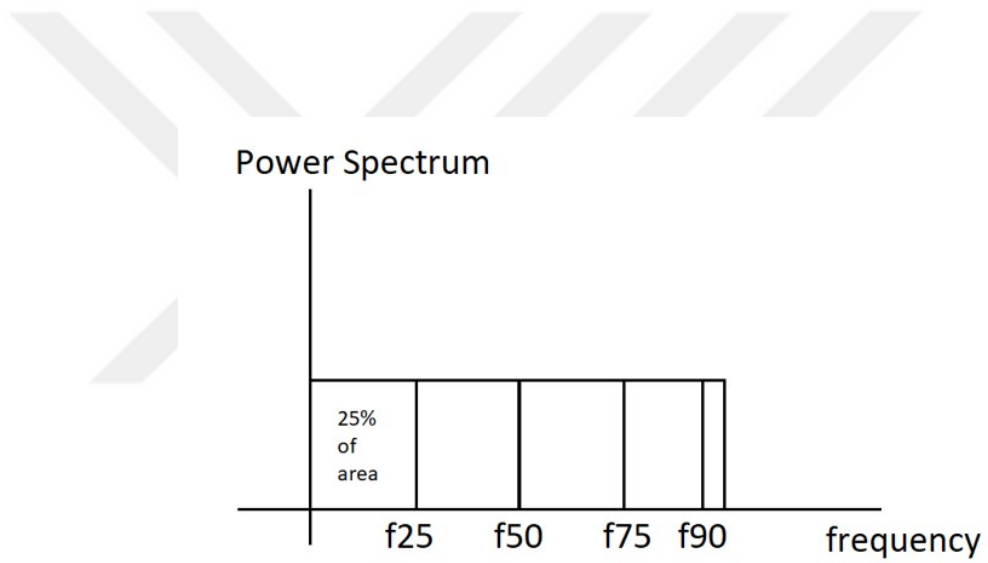


Figure 6.1. The Percentile Frequencies of a PSD.

7. EXPERIMENTS AND RESULTS

There are 12 measurements with 3 healthy subjects that are listed in Table 7.1, and the results of 3 of them are shown in Figure 7.1, Figure 7.2 and Figure 7.3.

Table 7.1. The Information Table of Health Subjects.

Subject Name	Sex	Age	Smoker/Non-Smoker	Weight	Height
Measurement 1	Female	60	Smoker	80	165
Measurement 2	Male	31	Non-Smoker	88	186
Measurement 3	Male	70	Non-Smoker	110	175

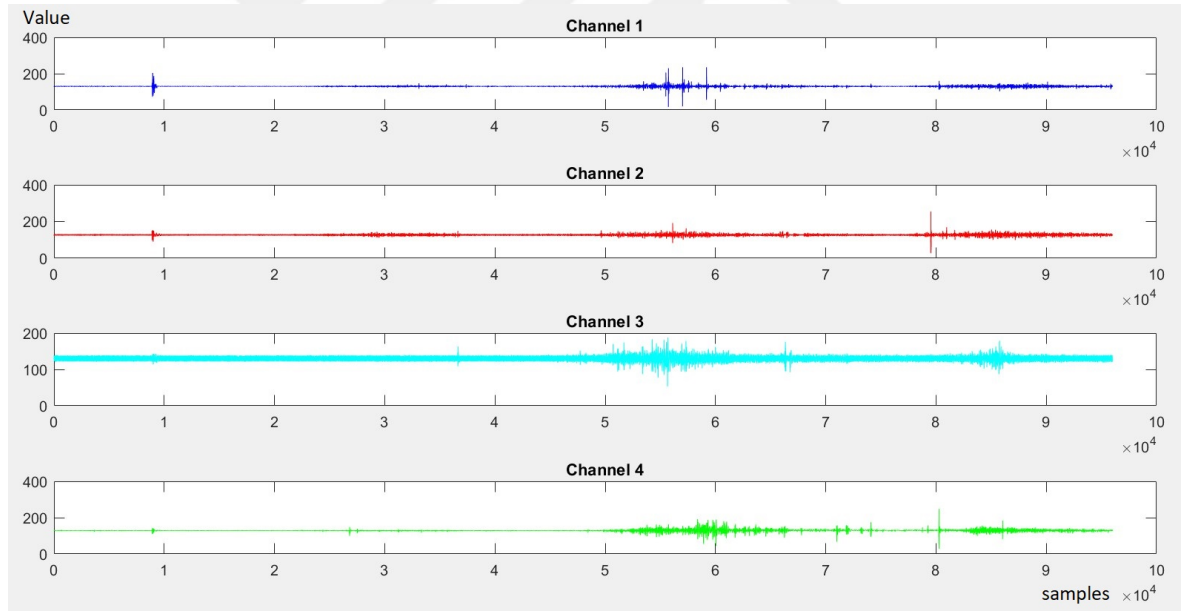


Figure 7.1. The Respiratory Sound Waveforms of 4 Channels of Measurement 1.

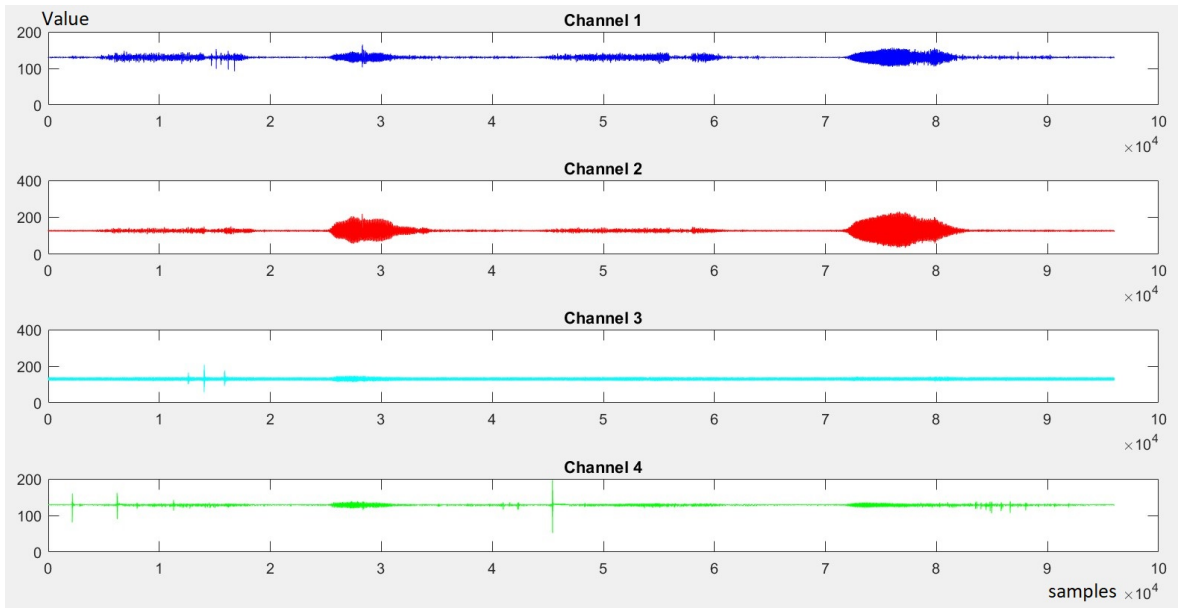


Figure 7.2. The Respiratory Sound Waveforms of 4 Channels of Measurement 2.

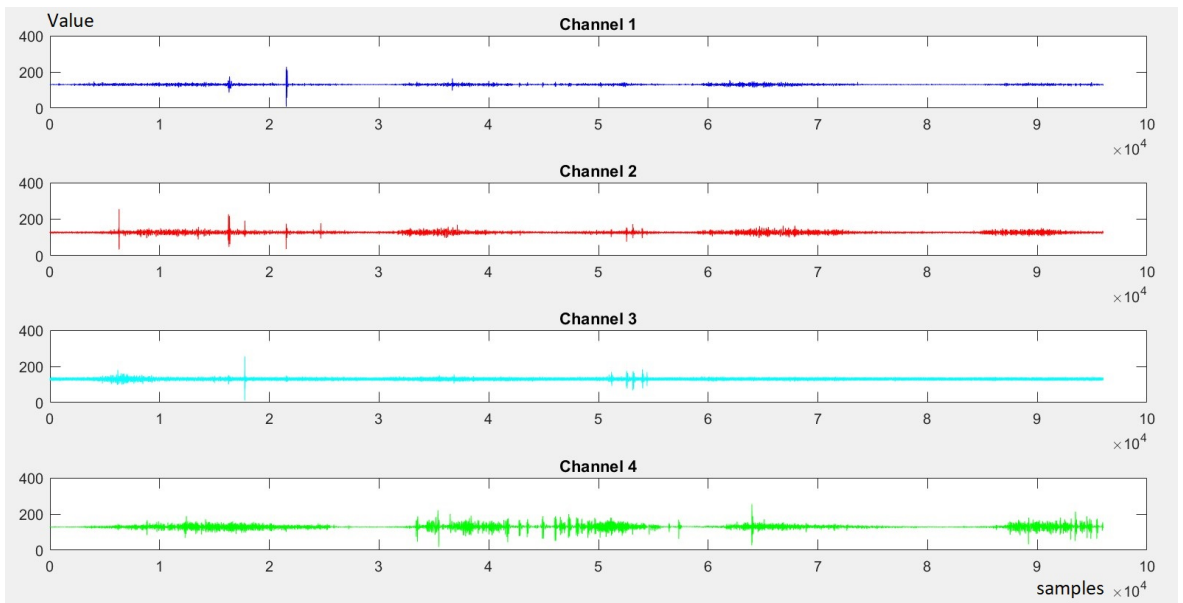


Figure 7.3. The Respiratory Sound Waveforms of 4 Channels of Measurement 3.

Table 7.2. Percentile Frequencies Table of Channel 1 for Each Measurements.

CH1	$f_{25}(Hz)$	$f_{50}(Hz)$	$f_{75}(Hz)$	$f_{90}(Hz)$
Measurement 1	23	82	180	316
Measurement 2	16	44	138	297
Measurement 3	16	39	109	256

Table 7.3. Percentile Frequencies Table of Channel 2 for Each Measurements.

CH2	$f_{25}(Hz)$	$f_{50}(Hz)$	$f_{75}(Hz)$	$f_{90}(Hz)$
Measurement 1	60	142	279	409
Measurement 2	51	129	295	423
Measurement 3	28	87	232	393

Table 7.4. Percentile Frequencies Table of Channel 3 for Each Measurements.

CH3	$f_{25}(Hz)$	$f_{50}(Hz)$	$f_{75}(Hz)$	$f_{90}(Hz)$
Measurement 1	95	215	369	412
Measurement 2	119	251	394	457
Measurement 3	95	223	375	446

According to the results of Measurement 1, 2 and 3, the percentile frequencies on Table 7.2, Table 7.3, Table 7.4 and Table 7.5 are consistent with the results of healthy subjects in [8].

The differences between channels are the results of the positions of channels on back side on the chest, and also the component variances on each capsule board and the contact problems between the body of subjects and capsule boards.

Table 7.5. Percentile Frequencies Table of Channel 4 for Each Measurements.

CH4	$f_{25}(Hz)$	$f_{50}(Hz)$	$f_{75}(Hz)$	$f_{90}(Hz)$
Measurement 1	36	92	205	324
Measurement 2	43	123	290	419
Measurement 3	26	58	133	257

8. CONCLUSION

In this thesis, a complete wearable device has been designed, produced with all physical components and also tested. While everything around us is being digital, auscultation is not going to be the same as today in the near future. Therefore, it is an innovative and useful device for both patients and medical professionals.

In the wearable part, two options are completed with not only at design stage but also at their component research for adjustable localization of capsules and also production of its textile. Corset and pillow options are practical, however their usability can be enhanced by finding adhesive components for better fit of microphone capsules on the back side of the chest of patients. There is also a mechanical enclosure design and production in this thesis, that can be designed again as smaller than the previous one.

In electronic design, two different 4-layer PCBs are designed with analog pre-processing circuitry that includes voltage references, band pass filters, instrumentation amplifiers and power management, and also microcontroller based digital system design with various peripheral connections such as Bluetooth, memories, pulse oximeter and various sensors. Besides designing circuits, their soldering, testing and prototyping are completed at the end of the thesis.

After mechanical and electronics parts, embedded software and mobile application are completed. While connecting the wearable device via Bluetooth connectivity from a computer, the respiratory and cardiac signals of all channels can be drawn and shown on MATLAB. In addition to this, there is an Android application that visualizes percentile frequencies at the end of the record session that also communicates with the wearable device via Bluetooth connectivity.

In addition to the data acquisition capabilities of the system, percentile frequencies are calculated on the embedded side. In fact, it is one of the significant features of the system because of the fact that by using large memory options of the device, every respiratory and cardiac sounds can be stored on microSD card with patient IDs. Then, using k-NN classification, the device can make primitive decision making via updating itself with new measurements.

In conclusion, after adding pulse oximeter, accelerometer and classification features mentioned above, the abilities of the device will be extended and become a complete device for data acquisition and classification for both of the respiratory and cardiac sounds.

REFERENCES

1. *Auscultation*, *Wikipedia Website*, <https://en.wikipedia.org/wiki/Auscultation>, accessed in July 2019.
2. *Stethoscope*, *Wikipedia Website*, <https://en.wikipedia.org/wiki/Stethoscope>, accessed in July 2019.
3. Pasterkamp H., S.S. Kraman and G.R. Wodicka, "Advances Beyond the Stethoscope", *American Journal of Respiratory and Critical Care Medicine*, Vol. 156, pp. 974-987, September 1997.
4. Vanucci L., J. E. Earis, P. Heliöstö, B. M. G. Cheetham, M. Rossi, A. R. A. Sovijärvi and J. Vanderschoot, "Capturing and Preprocessing of Respiratory Sounds", *European Respiratory Review*, Vol. 10, No. 77, pp. 616-620, 2000.
5. Ertel P. Y., Lawrence M., Brown R. K. and Stern A. M., "Stethoscope Acoustics: II. Transmission and Filtration Patterns", *Circulation*, Volume XXXIV, November 1966.
6. Sovijärvi A. R. A., F. Dalmaso, J. Vanderschoot, L. P. Malmberg, G. Righini and S. A. T. Stoneman, "Definition of Terms for Respiratory Sounds", *European Respiratory Review*, Vol. 10, No. 77, pp. 559-610, 2000.
7. Şen, İ., A Multi-Channel Device for Respiratory Sound Data Acquisition and Transient Detection, Master's Thesis, Boğaziçi University, 2005.
8. Cini, U., A DSP Processor Based Pulmonary Pathology Localization Instrument Using Lung Sounds, Master's Thesis, Boğaziçi University, 2003.
9. Xian-ting, T., Zhi-dong, Z., Heart Sound Acquisition Based on PDA and Bluetooth, 4th International Conference on Biomedical Engineering and Informatics (BMEI),

- 2011.
10. *STM32F7x7*, *ST Microelectronics Website*, <https://www.st.com/en/microcontrollers-microprocessors/stm32f7x7.html>, accessed in July 2019.
 11. *RN42/RN42N Datasheet*, *Microchip Website*, <http://ww1.microchip.com/downloads/en/DeviceDoc/50002328A.pdf>, accessed in July 2019.
 12. *Conductive Rubber Cord Stretch Sensor*, *Adafruit Website*, <https://www.adafruit.com/product/519>, accessed in July 2019.
 13. *MAX30100 Datasheet*, *Maxim Integrated Website*, <https://www.maximintegrated.com/en/products/sensors/MAX30100.html>, accessed in July 2019.
 14. Franco S., *Design with Operational Amplifiers and Analog Integrated Circuits*, 3rd Ed., McGraw-Hill, 2002.
 15. *Analog Filters*, *Analog Devices Website*, <https://www.analog.com/media/en/training-seminars/design-handbooks>, accessed in July 2019.
 16. *Complex DFT and FFT Algorithm*, *Embedded System Engineering Website*, <http://embeddedsystemengineering.blogspot.com/2016/06/>, accessed in July 2019.
 17. Ulukaya S., Serbes G., Şen İ., Kahya Y., " Akciğer Solunum Seslerinin Spektral Öznitelikler ile Sınıflandırılması", Vol 22, Issue 2, 711-716, *Journal of Natural and Applied Sciences*, Süleyman Demirel University, 2018.
 18. *POM-2245L-C33-R Datasheet*, *PUI Audio Website*, <http://www.puiaudio.com/pdf/POM-2245L-C33-R.pdf>, accessed in July 2019.

APPENDIX A: TECHNICAL DRAWING OF THE MICROPHONE CAPSULES

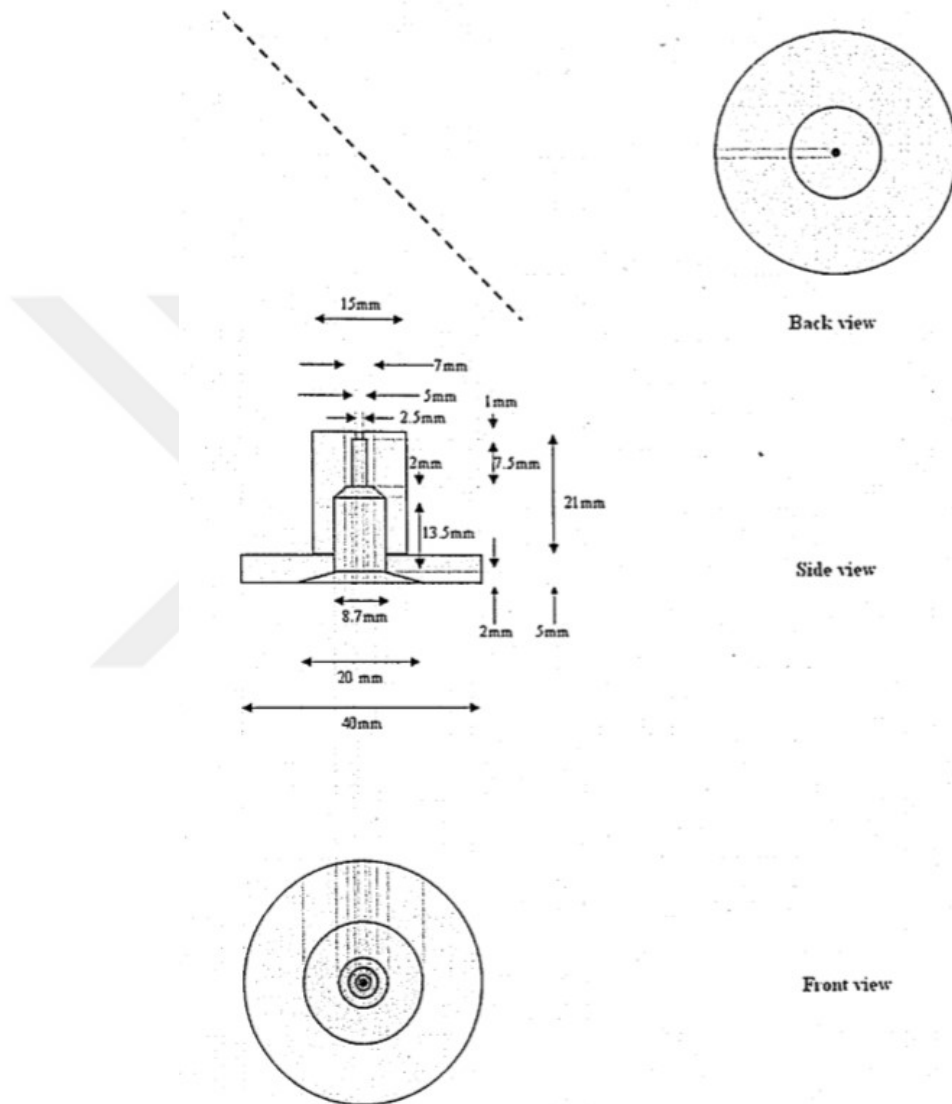


Figure A.1. Technical Drawing of the Microphone Capsules.

APPENDIX B: FAST FOURIER TRANSFORM ALGORITHM [16]

```
void fft()
{
    int nm1 = N - 1;
    int nd2 = N / 2;
    int m = log10(N) / log10(2);
    int j = nd2;
    int k;
    int le, le2;
    float ur, ui, sr, si;
    int jm1;
    int ip;
    float tr, ti;
    // Bit reversal sorting
    for (int i = 1; i <= N-2; i++)
    {
        if (i >= j) goto a;
        tr = REX[j];
        ti = IMX[j];
        REX[j] = REX[i];
        IMX[j] = IMX[i];
        REX[i] = tr;
        IMX[i] = ti;
        a:
        k = nd2;
        b:
        if (k > j) goto c;
        j -= k;
        k /= 2;
        goto b;
        c:
```

```

    j += k;
} // Loop each stage
for (int l = 1; l <= m; l++)
{
    le = pow(2, l);
    le2 = le / 2;
    ur = 1;
    ui = 0;
    // Calculate sine and cosine values
    sr = cos(PI/le2);
    si = -sin(PI/le2);
    // Loop for each sub DFT
    for (int j = 1; j <= le2; j++)
    {
        jm1 = j - 1;
        // Loop for each butterfly
        for (int i = jm1; i <= nm1; i += le)
        {
            ip = i + le2;
            tr = REX[ip]*ur - IMX[ip]*ui;
            ti = REX[ip]*ui + IMX[ip]*ur;
            REX[ip] = REX[i] - tr;
            IMX[ip] = IMX[i] - ti;
            REX[i] = REX[i] + tr;
            IMX[i] = IMX[i] + ti;
        }
        tr = ur;
        ur = tr*sr - ui*si;
        ui = tr*si + ui*sr;
    }
}
}

```

APPENDIX C: THE DATASHEET OF POM-2245L-C33R MICROPHONE

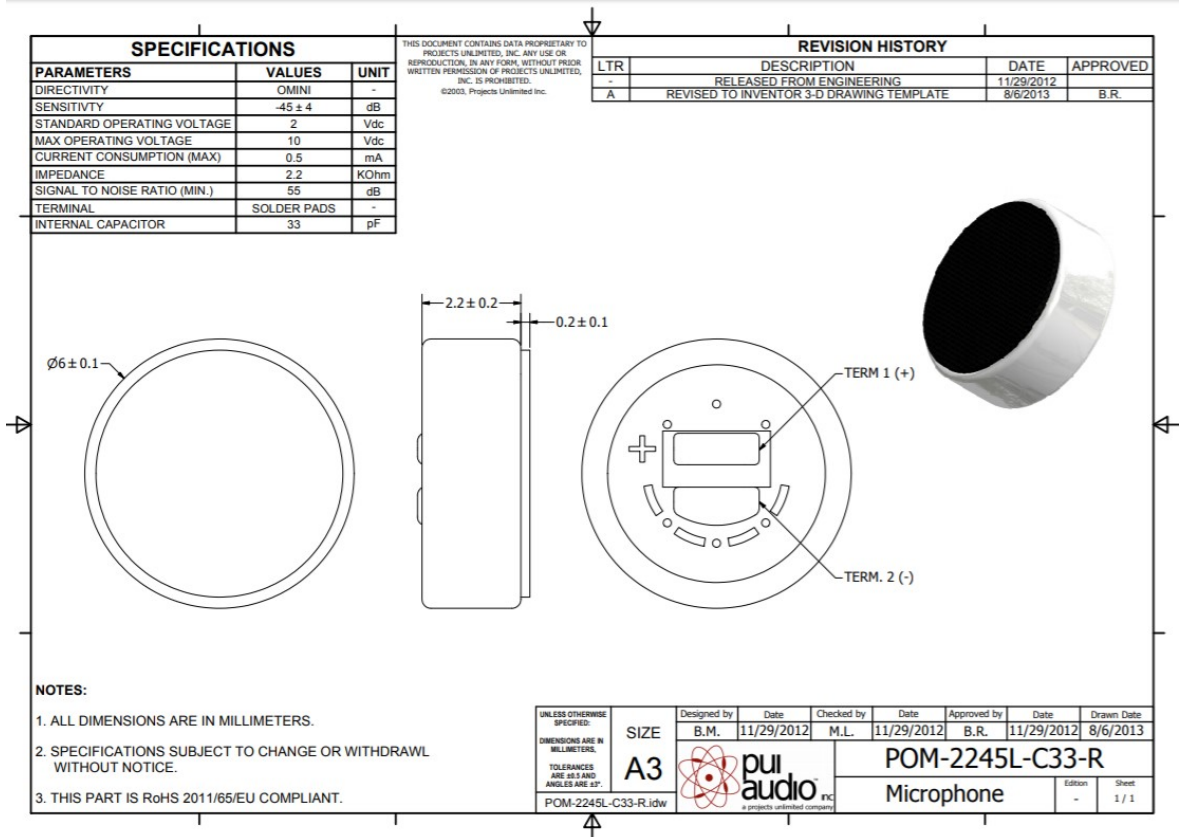


Figure C.1. The Datasheet of POM-2245L-C33-R Electret Microphone [18].

APPENDIX D: THE COMPONENT LIST OF THE MAIN BOARD

Table D.1. The IC Table of the Main Board.

IC	Name	Package
U1,U7	MCP73812	SOT-23-5
U2,U8	STMPS2151	SOT-23-5
U3	STM32F777	LQFP144
U4,U5,U6	TPS73633	SOT23-5
U9	RN42	RN42-MODEL
U10	SPBT3	SPBT3-MODEL
U11	FT232RL	SSOP28
U12	IS62WV10248	44TSOP-2
U13	S25FL128S	8-WSON
U14	LM4875	SO8
U15	NX3L4051	TSSOP16
U16	CD4511B	TSSOP16
U17	REF2033	SOT-23-5
U18	TS3A24159	VSSOP10
U19,U23,U24	AD8226	SO8
U20,U21,U22	OPA4342	SO14
U25	MCP4161	SO8

Table D.2. The Resistor Table of the Main Board.

Resistor	Value	Package
R1	220k Ω	603
R2	330k Ω	603
R3,R6	2k Ω	603
R7,R8,R9,R10,R11,R12,R14,R15,R16,R17	0.1 Ω	603
R18,R22,R23,R25,R32,R39,R41,R42,R45,R46	0.1 Ω	603
R55,R57,R58,R91,R92,R94,R102,R103,R104	0.1 Ω	603
R114,R115,R116,R117	0.1 Ω	603
R4,R5,R13,R19,R20,R21,R34,R38,R54,R70	10k Ω	603
R81,R82,R83,R84,R85,R86,R87,R88,R89	10k Ω	603
R90,R100,R101,R106,R107,R118	10k Ω	603
R24,R26,R113	4.7k Ω	603
R27,R28,R29,R30,R31,R33	47k Ω	603
R35,R36,R37	470 Ω	603
R40,R44,R62,R63,R96,R97,R111,R112	100k Ω	603
R43	150 Ω	603
R47,R48,R49,R50,R51,R52,R53,R59	220 Ω	603
R56	2.2k Ω	805
R60,R61,R95,R105,R109,R110	3.9k Ω	603
R64,R77	18k Ω	603
R65	75k Ω	603
R66,R76	39k Ω	603
R67	27k Ω	603
R68,R69,R80	33k Ω	603
R72	100 Ω	603
R73	11k Ω	603
R74,R78	12k Ω	603
R75	36k Ω	603
R79	15k Ω	603

Table D.3. The Capacitor Table of the Main Board.

Capacitor	Value	Package
C1,C76,C111,C122,C125	10nF	603
C2,C3,C4,C5,C10,C11,C27,C29,C30,C31,C53	1uF	603
C56,C59,C64,C66,C78,C127,C131	1uF	603
C6,C19,C24,C26,C32,C57,C58,C67	10uF	805
C7,C8,C9,C12,C15,C16,C17,C18,C20,C21,C25	100nF	603
C28,C33,C34,C35,C36,C37,C38,C39,C40,C41	100nF	603
C42,C43,C44,C45,C50,C51,C52,C54,C55,C62	100nF	603
C63,C65,C69,C74,C75,C77,C80,C81,C82,C83	100nF	603
C84,C85,C86,C87,C92,C97,C99,C101,C102	100nF	603
C103,C104,C105,C106,C107,C108,C109	100nF	603
C110,C116,C117,C123,C124,C126,C129	100nF	603
C13	4.7uF	603
C14,C79,C128	3300uF	ELEC-RAD50M
C22,C23	2.2uF	603
C46,C47	9pF	603
C48,C49	8pF	603
C60	100uF	ELEC-RAD20M
C61	220nF	805
C68,C70,C96,C112,C115,C118,C119	1nF	603
C71,C72,C113,C114,C120,C121	22nF	603
C73	10nF	805
C90	8.2nF	603
C91	5.6nF	603
C93	1.2nF	603
C94,C100	3.9nF	603
C95	27nF	603
C98	3.3nF	603
C132	2700uF	ALI-POLY-CAP

APPENDIX E: THE COMPONENT LIST OF THE CAPSULE BOARD

Table E.1. The IC Table of the Capsule Board.

IC	Name	Package
U1	AD8226	SO8
U2,U3,U5	OPA4342	SO14
U4	TS3A24159	VSSOP10
U6	IIS2DH	LGA-12
U7	TPS73633	SOT-23-5
U8	REF2033	SOT-23-5
U9	MCP3201	SO8
U10	MCP4161	SO8

Table E.2. The Resistor Table of the Capsule Board.

Resistor	Value	Package
R1	220 Ω	603
R2,R3	3.9k Ω	603
R4,R5	100k Ω	603
R6,R18	12k Ω	603
R7,R36	2.2k Ω	603
R8,R17	18k Ω	603
R9	75k Ω	603
R10,R16	39k Ω	603
R11	27k Ω	603
R12,R20,R23	33k Ω	603
R13,R24,R26,R32,R33,R34	0.1 Ω	603
R14	11k Ω	603
R15	36k Ω	603
R19	15k Ω	603
R21,R22,R25,R27,R28,R29,R30,R31	10k Ω	603
R35	1 Ω	603

Table E.3. The Capacitor Table of the Capsule Board.

Capacitor	Value	Package
C1,C65	10nF	603
C2,C3,C24	1nF	603
C4,C5	22nF	603
C6,C7,C8,C9,C10,C11,C12,C13,C14,C15,C18	10uF	805
C23,C26,C27,C30,C32,C34,C35,C36,C37,C38	100nF	603
C39,C40,C41,C42,C43,C44,C50,C52,C58,C63	100nF	603
C64,C66,C68	100nF	603
C16	8.2nF	603
C17	5.6nF	603
C19	1.2nF	603
C20,C21	3.9nF	603
C22	3.3nF	603
C25	27nF	603
C28,C29,C33,C69,C71	1uF	603
C31,C45	10uF	603
C46	1nF	603
C70	3300uF	ELEC-RAD50M